JVI Accepted Manuscript Posted Online 27 November 2019
J. Virol. doi:10.1128/JVI.01925-19
Copyright © 2019 American Society for Microbiology. All Rights Reserved.

JVI

Nucleocapsid protein recruitment to replication-transcription complexes plays a crucial role in coronaviral life cycle

Yingying Cong[a], Mustafa Ulasli[b], Hein Schepers[a], Mario Mauthe[a], Philip V'kovski[c,d], Franziska Kriegenburg[a], Volker Thiel[c,d], Cornelis A.M. de Haan[e], Fulvio Reggiori[a,b#]

[a]Department of Biomedical Sciences of Cells & Systems, University Medical Center Groningen, University of Groningen, A. Deusinglaan 1, 9713 AV Groningen, The Netherlands

[b]Department of Cell Biology, University Medical Center Utrecht, Heidelberglaan 100, 3584 CX Utrecht, The Netherlands

[c]Institute of Virology and Immunology IVI, Bern, Switzerland

[d]Department of Infectious Diseases and Pathobiology, Vetsuisse Faculty, University of Bern, Bern, Switzerland

[e]Virology Division, Department of Infectious Diseases & Immunology, Faculty of Veterinary Medicine, Utrecht University, Utrecht, The Netherlands

[#]Correspondence: f.m.reggiori@umcg.nl

Running title: CoV N-nsp3 interaction in coronaviral infection

ABSTRACT

Coronaviruses (CoV) nucleocapsid N proteins are key in incorporating the genomic RNA into the progeny viral particles. In infected cells, N proteins are present at the replication-transcription complexes (RTCs), the sites of CoV RNA synthesis. It has been shown that N proteins are important for viral replication and that the one of mouse hepatitis virus (MHV), a commonly used CoV model virus, interacts with non-structural protein 3 (nsp3), a component of the RTCs. These two aspects of CoV life cycle, however, have not been linked. We found that the MHV N protein binds exclusively to nsp3 but not with other RTCs components using a systematic yeast two-hybrid approach, and identified two distinct regions in the N protein that redundantly mediates this interaction. A selective N protein variant carrying point mutations in these two regions fail to bind nsp3 *in vitro*, resulting in an inhibition of its recruitment to the RTCs *in vivo*. Furthermore, opposite to the wild type N protein, this N protein variant impairs the stimulation of gRNA and viral mRNA transcription *in vivo* and *in vitro*, which in turn leads to an impairment in MHV replication and progeny production. Altogether, our results show that N protein recruitment to RTCs, via binding to nsp3, is an essential step in CoV life cycle as it is critical for optimal viral RNA synthesis.

IMPORTANCE

Coronaviruses (CoV) have been regarded for a long time as a relatively harmless pathogen for humans. Two severe respiratory tract infection outbreaks caused by SARS-CoV and MERS-CoV, however, have caused high pathogenicity and mortality rates in humans. This highlighted the relevance of being able to control CoV infections. We used a CoV model virus, mouse hepatitis virus (MHV), to investigate the importance of the recruitment of nucleocapsid (N)

protein, a central component of CoV virions, to intracellular platforms where CoV replicate, transcribe and translate their genomes. By identifying the principal binding partner at these intracellular platforms and generating a specific mutant, we found that N protein recruitment to these locations is crucial in promoting viral RNA synthesis. Moreover, blocking this recruitment strongly inhibits viral infection. Thus, our results explain both an important aspect of CoV life cycle and reveal an interaction between viral proteins that could be targeted in antiviral therapies.

KEYWORDS

Coronavirus, nucleocapsid N protein, replication-transcription complexes, viral mRNA synthesis

JVI

INTRODUCTION

Coronaviruses (CoV) is a family of viruses that cause numerous pathologies in humans and other mammals, including respiratory, enteric, hepatic and neurological diseases, with varying severities (1-3). CoV are subdivided into four genera: *Alphacoronavirus*, *Betacoronavirus* (beta-CoV), *Gammacoronavirus* and *Deltacoronavirus* (4). Human pathogens that can be lethal, such as the Severe Acute Respiratory Syndrome (SARS)- and Middle East Respiratory Syndrome (MERS)-CoV, belong to the beta-CoV genus (1-3). Mouse hepatitis virus (MHV), which is also part of the beta-CoV genus, is considered the prototype virus for the study of the CoV infection mechanism.

CoV are enveloped viruses with single-stranded positive-sense RNA genomes. Their genomes are approximately 30 kb and encode for the structural proteins, accessory proteins and contain two overlapping open reading frames, ORF1a and ORF1b, which are translated into two large polyproteins, pp1a and pp1ab. These polyproteins are processed into 15 or 16 non-structural proteins (nsp) by multiple viral proteinase activities present in their sequence (2). Collectively, nsp proteins form the replication and transcription complexes (RTCs), which play a crucial role in the synthesis of viral RNA (5-9). Immuno-fluorescence and electron microscopy studies have revealed that CoV RTCs proteins are localized onto membrane networks composed by convoluted membranes and double-membrane vesicles (DMVs), which are induced by the nsp themselves (7, 10-12). RTCs together with recruited host factors, copy the genome either continuously into a genome-length template (*i.e.*, replication) or discontinuously into the various subgenome-length minus-strand templates (*i.e.*, transcription). These minus-strands templates are used for the synthesis of new molecules of gRNA and subgenomic mRNAs (sgmRNA) (2, 5). The sgmRNA encode for both CoV structural and accessory proteins. CoV particles are formed by at least 4 structural proteins: the spike (S), the membrane (M), the envelope (E), and the nucleocapsid (N) protein. While the M, E and S proteins together with membranes derived from host organelles compose the virion envelope, the N protein binds the gRNA and allows its encapsidation into viral particles (13). Virions are formed by inward budding through the limiting membrane of the endoplasmic reticulum (ER), ER-Golgi intermediate compartment (ERGIC) and/or Golgi, and reach the extracellular milieu through the secretory pathway (2, 3).

CoV N proteins have three distinct and highly conserved domains, *i.e.*, the N-terminal domain (NTD or N1b), the C-terminal domain (CTD or N2b) and the N3 region (14) (Fig. 1A). The crystal structures of the N1b and N2b domains of the N protein from SARS-CoV, infectious bronchitis virus (IBV), human coronavirus 229E and MHV, show a similar overall topological organization (15-20). The charged N2a domain, which contains a stretch of amino acids rich in serine and arginine residues and known as the SR-rich region, links N1b and N2b (14) (Fig. 1A). N proteins form dimers, which asymmetrically arrange themselves into octamers via their N2b domains and further assemble into larger oligomeric structures that acquire either a loose or a more compact intertwined filament shape (19, 21, 22). This oligomerization occurs constitutively and it might provide a larger binding surface for the optimal entangling of the large gRNA, as the multimerizing N2b domains will form the core of the N protein filaments while the RNA-binding N1b domains will decorate their surface (20, 23, 24). The resulting N protein-gRNA ribonucleoprotein complexes are finally incorporated into the forming viral particles through interactions with the C-terminus of the M proteins (25).

CoV N protein plays a regulatory role in viral replication or transcription, a notion sustained by several studies showing that the N protein has RNA-binding and chaperone activities, and promote CoV gRNA replication (26-29). Phosphorylation of IBV, SARS-CoV and

JVI

MHV N protein allows to discriminate binding between viral and non-viral mRNA (30, 31). The SR-rich region appears to be the domain of CoV N proteins that is mostly modified by phosphorylation (32, 33). Interestingly, it has been revealed that a priming phosphorylation of Ser205 of MHV N protein and of Ser189 and Ser207 of SARS-CoV N protein by a so far unknown kinase, triggers the subsequent phosphorylation of several residue of the SR-rich region by the host glycogen synthase kinase-3 (GSK-3) (32). Phosphorylation by GSK-3 allows association of the RNA helicase DDX1 with N protein, which facilitates template read-through and enables the transition from discontinuous transcription of sgmRNA to continuous synthesis of longer sgmRNA and gRNA (32). Intriguingly, part of the N proteins localizes to RTCs and this peculiar distribution is already observed at the early stages of infection (34-37). In contrast to most of the nsp that appear to be static components of the RTCs (38), the N protein is dynamically associated with these structures leading to the idea that it could be recruited to RTCs to stimulate the synthesis and eventually entangle gRNA (39). Interestingly, it has been shown that MHV N protein interacts with nsp3 (40, 41), one of the components of the RTCs, but it remains unclear whether this interaction is required for the N protein recruitment to the RTCs. While co-transfection of N protein mRNA with MHV gRNA promotes viral replication, mRNAs encoding for N protein chimera that is not able to interact with nsp3 do not have the same pro-viral effect (40, 41). These observations indirectly indicate that N protein association to RTCs could have a relevant role in the CoV life cycle.

To unveil the recruitment mechanism and the function of the N protein at the RTCs, we have decided to investigate the molecular mechanism underlying the association of this protein to RTCs. The characterization of this interaction has allowed us to experimentally block it and thereby determine its relevance for CoV life cycle. We have found that N protein gets indeed recruited to the RTCs by interacting with nsp3. Using an *in vitro* binding approach, we show that regions in the N1b and N2a domains of MHV N protein mediate the binding to nsp3 in a gRNA-independent manner. Importantly, we identified and created specific N protein point mutants that block its binding to nsp3 *in vitro*, and found that this association is necessary for N protein recruitment and function at the RTCs *in vivo*. At the RTCs, the nsp3-mediated recruited N protein is required for the stimulation of gRNA replication and sgmRNA transcription. Indeed, the inhibition of N protein-nsp3 interaction severely impairs viral replication and egression. Altogether, our data demonstrate that N protein interaction with nsp3 is a critical step for the MHV replication and its targeting could represent a valid anti-coronaviral therapy.

JVI

RESULTS

Nsp3 is the principal binding partner of the N protein within the RTCs

N protein interacts with nsp3 (40, 41) and therefore we hypothesized that it is recruited to the RTCs by binding one or more nsp. We initially determined which components of the RTCs interact with the N protein; in particular whether other nsp proteins, apart from nsp3, also bind the N protein using yeast two-hybrid (Y2H) assay (42). To this aim, the N protein of MHV and all 16 nsp proteins were cloned into the vector carrying the activation domain (AD) and the DNA binding domain (BD) of the yeast Gal4 transcription factor, respectively (42). Each plasmid encoding for a BD-nsp fusion protein was transformed together with the one expressing the AD-N chimera into the Y2H test strain and growth of the co-transformed cells on a medium lacking histidine was used to assess interaction. As shown in Fig. 1B, this approach revealed that MHV N protein mainly binds to nsp3 in agreement with the previous findings (40, 41, 43) and to a far lesser extent also to nsp4. Since this potential interaction was only detected in one replicate, we did not investigate this further.

Previous analyses have revealed that the large cytosolic N-terminal part of nsp3 from amino acid 1 to 233, *i.e.*, nsp3^{N}, is important for interaction with the N protein (40, 41). In these studies, however, purified nsp3^{N} was incubated with cell extracts from MHV-infected cells. As a result, this approach cannot exclude that N protein interacts indirectly with nsp3, *i.e.*, via either a cellular or another viral protein, and therefore a different factor could be involved in N protein recruitment to the RTCs. Thus, we first examined whether the N protein and nsp3 bind directly using *in vitro* binding experiments as well. The nsp3^{N} fragment was fused to glutathione transferase (GST), expressed in *E. coli* and purified using sepharose bead-conjugated glutathione (GSH). To prove that our purified nsp3^{N} fragment still retains its overall conformation, GST or

JVI

GST-nsp3^N were first incubated with cell extracts obtained from non-infected and MHV-infected LR7 cells. As shown in Fig. 1C and consistently with the literature (41), the N protein specifically binds to GST-nsp3^N but not to GST alone. We also tested whether association with RNA was influencing N protein binding to nsp3^N because this parameter could be relevant for the following-up *in vitro* studies with recombinant proteins. Therefore, cell extracts from infected cells were treated with RNase A or with this enzyme plus a specific RNase A inhibitor, before being incubated with GST-nsp3^N or GST. Importantly, removal of RNA did not alter N protein interaction with nps3^N (Fig. 1C).

Next, we fused N protein with 6×His tag and expressed this fusion protein in *E. coli* before preparing bacterial cell extracts and incubating them with either GST or GST-nsp3^N. As shown in Fig. 1D, recombinant N protein specifically binds to purified GST-nsp3^N but not GST. Altogether, these experiments show that nsp3, through its N-terminus, is the only RTC component that binds directly to the N protein and that this binding does not require N protein association to RNA.

Two domains are required for N protein interaction with nsp3

To unravel the recruitment mechanism of N protein to the RTCs through binding via nsp3, we dissected how N protein interacts with nsp3. We generated a series of C-terminal truncated variants of the N protein and assessed their interaction with nsp3 using the Y2H system to identify the nsp3-binding regions of the N protein (Fig. 2A). Consistent with previous reports (40, 41, 44), we pinpointed one binding region to the N2a domain, between the amino acids 233 and 250, which contains the SR-rich region. To elaborate further on this, we generated 3 truncated forms, *i.e.*, N1a-N1b/NTD (1-194aa), N2a (195-257aa) and N2b-N3/CTD (258-454aa)

JVI

(Fig. 1A). These truncations were fused with the 6×His tag and expressed in *E. coli* before preparing bacterial cell extracts, which were then incubated with either GST or GST-nsp3^{N}. As expected and shown in Fig. 2B, none of the fusion proteins interacted with GST. In contrast, binding between GST-nsp3^{N} and 6×His-N1a-N1b was detected as previously suggested (45), but not with 6×His-N2a and 6×His-N2b-N3. As interaction between nsp3 and N2a has previously been reported (40, 41) but shown to possess a weak affinity (44), we repeated the pull-down experiments between GST-nps3^{N} and 6×His-N2a, and exposed the western blot membranes for a longer time (Fig. 2C). This approach allowed detecting the binding between nps3^{N} and N2a, in agreement to our Y2H analysis of the truncated N proteins (Fig. 2A). This result shows that motifs in 2 different regions of the N protein, *i.e.*, N1a-N1b and to a much smaller extent N2a, are mediating its binding to nsp3.

In order to identify these motifs and study their relationship, we aligned the amino acids sequences of the N1-N2a segment of the N protein from different beta-CoV and examined their distribution on the 3D structure of the MHV N1-N2a domain (24). As highlighted in Fig. 3A, we found six stretches of amino acids that were both conserved and on the surface of the N1-N2a, thus making them available for an interaction. Four of these amino acid stretches were localized in the N1 region and two in the N2a fragment. We mutated the conserved polar and charged amino acids into alanines, and the conserved nonpolar amino acids into aspartates, in each one of these different sequences creating mutated versions of the 6×His-tagged N protein truncations: N2a^{m1} (amino acids 195 to 257, with L240E, V241E and L242E mutations), N2a^{m2} (amino acids 195 to 257, with S197A, R202A, S203A and S205A mutations), N1^{m3} (amino acids 1 to 194, with T73A, Q74A and K77A mutations), N1^{m4} (amino acids 1 to 194, with K101A, Y103A and W104A mutations), N1^{m5} (amino acids 1 to 194 with R109A, R110A and K113A mutations) and

JVI

$N1^{m6}$ (amino acids 1 to 194, with F128A, Y129A, Y130A and T133A mutations) (Fig. 3A). Of note, the S205A change in the $N2a^{m2}$ variant alters the priming site essential for SR-rich region phosphorylation by host cell GSK3 (32, 46). Cell extracts obtained from *E. coli* expressing these constructs were incubated with either GST or GST-$nsp3^{N}$. Although $N1^{m3}$ and $N1^{m5}$ bound GST-$nsp3^{N}$ with the same affinity as wild type N1, we found that the other mutated truncations displayed a strong reduction in the interaction with GST-$nsp3^{N}$ (Fig. 3B). We concluded that amino acids at positions 101 to 104 and 129 to 133, and 194 to 202 and 240 to 242, play a role in the interaction between nsp3 with N1 and N2a, respectively (Fig. 3B). This result also revealed that the SR-rich region that gets phosphorylated *in vivo* is not important for N protein binding to nsp3.

This finding indicated two possible scenarios. In the first, the two identified nsp3 binding domains act cooperatively and disruption of one of them is sufficient to abolish nsp3-N protein interaction. In the second, the two identified nsp3 binding domain are redundant and mutation of only one of them does not affect the association between nsp3 and N protein. Thus, to determine whether the single mutations in N1 or N2a are sufficient to block N1-N2a interaction with $nsp3^{N}$, we expressed the N1-$N2a^{m1}$, N1-$N2a^{m2}$, N1-$N2a^{m4}$ or N1-$N2a^{m6}$ variants in *E. coli* before to incubate bacterial extracts with either GST or GST-$nsp3^{N}$. As shown in Fig. 3C, all constructs specifically bind GST-$nsp3^{N}$ with the same affinity as wild type N1-N2a. This finding showed that the binding of MHV N protein to nsp3 is not mediated by a single domain and therefore the domains might be redundant in the binding function as contemplated in the second scenario.

Consequently, we next assessed whether the combined mutations in the critical amino acids of N1b and N2a could block N protein-nsp3 interaction. To this aim, we expressed full-

JVI

length N, N^{m4m1}, N^{m6m1}, N^{m4m2} or N^{m6m2} in *E. coli* and incubated bacterial extracts with either GST or GST-$nsp3^N$. Although N^{m4m2} and N^{m6m2} were still able to interact with $nsp3^N$, N^{m4m1} and N^{m6m1} displayed a strong reduction in their binding to $nsp3^N$ (Fig. 4A). This finding shows that two different regions mediate MHV N protein binding to nsp3. From here, we continued with the analysis of the N^{m4m1} and N^{m6m1} mutants to specifically study the N protein-nsp3 interaction.

The nsp3-binding domains of the N protein are not involved in its self-assembly and oligomerization

We and others have recently shown that CoV N proteins form oligomers constitutively (22, 23). Therefore, a possible scenario that could not be excluded a priori was that the introduced mutations in the N protein were affecting its organization in oligomers, which in turn may indirectly impair binding to nsp3. To investigate whether the mutated N proteins that showed reduced nsp3 binding, *i.e.*, N^{m4m1} and N^{m6m1} (Fig. 4A), have a defect in self-interaction, we analyzed their self-binding. Bacterial extract from *E. coli* expressing 6×His-tagged N, N^{m4m1} or N^{m6m1} were incubated with GST or GST-N protein. As shown in Fig. 4B, 6×His-N, 6×His-N^{m4m1} and 6×His-N^{m6m1} proteins specifically interact with GST-N protein.

To ascertain whether N^{m4m1} and N^{m6m1} proteins are also able to oligomerize, purified 6×His-N, 6×His-N^{m4m1} and 6×His-N^{m6m1} were resolved on a density glycerol gradient to determine the size of the oligomers that they form (23). Wild type N protein was mainly detected in fractions 4-6 as expected (Fig. 4D) (23). The distribution of the N^{m4m1} oligomer over the gradient differed slightly than the wild type, *i.e.*, the signal was mainly present in fractions 6-7, suggesting that it assembles predominately in larger oligomers. Importantly, the oligomerization

JVI

of N^{m6m1} variant was similar to that of the N protein as it was mainly detected in fractions 4-7 (Fig. 4C and D).

These results show that the regions involved in MHV N protein binding to nsp3 are not relevant for its oligomerization.

Nsp3 mediates N protein recruitment to RTCs

To establish whether the inability of the N protein to interact with nsp3 leads to an altered subcellular localization over the course of an infection, we first attempted to generate mutant MHV strains using two different approaches. First, we opted to generate recombinant MHV expressing an additional copy of GFP-tagged N or N^{m6m1} by inserting the coding sequence of these two fusion proteins into the viral locus of the nonessential hemagglutinin-esterase gene (39). The N^{m6m1} mutant was chosen because it oligomerizes similarly to the wild type N protein (Fig. 4D). We tried three times to generate an MHV-N^{m6m1}-GFP chimeric strain using this approach but although we obtained the control MHV-N-GFP strain at each time, we were unable to recover the mutant virus. Second, we turned to the vaccinia virus-based reverse genetics system to introduce the N^{m6m1} mutation in the viral N locus (47). With this approach as well, the wild type strain but not the mutant one was obtained in two attempts. As genomic expression of N^{m6m1} appeared to be lethal for the virus, we decided to opt for a different strategy. We expressed mCherry, mCherry-N or mCherry-N^{m6m1} fusion proteins in mouse LR7 cells before exposing them to MHV. mCherry, mCherry-N and mCherry-N^{m6m1} were homogenously distributed in the cytoplasm in non-infected cells (not shown). In contrast, MHV-infected cells displayed numerous distinct cytoplasmic puncta that were positive for both nsp2 and nsp3 (not shown); these puncta have been previously shown to represent RTCs (39). Interestingly, wild type

JVI

mCherry-N but not mCherry-N^{m6m1} or mCherry alone, was recruited to these nsp2/3-positive RTCs (not shown).

The low transfection efficiency of mouse LR7 cells (around 10%-15%), however, did not allow examining a sufficiently large number of cells that were both infected and expressing the analyzed chimeras for quantification. We therefore decided to turn to the human HeLa-CEACAM1a cell line, which expresses the MHV cell receptor CEACAM1a and it is highly transfectable (48). As expected, the GFP, GFP-N and GFP-N^{m6m1} constructs were efficiency transfected into HeLa-CEACAM1a cells as around 80% of the cells displayed the fluorescent signal. In agreement with the results obtained with LR7 cells, GFP, GFP-N and GFP-N^{m6m1} fusion proteins were homogenously distributed throughout the cytoplasm (Fig. 5A) and MHV infection caused a redistribution of GFP-N to the nsp2/nsp3-positive RTCs (Fig. 5A, fifth row). This observation confirmed that ectopically expressed GFP-tagged N protein behaves like the one encoded by the viral gRNA over the course of an infection. Surprisingly, we found that a large number of cells expressing GFP-N^{m6m1} did not display nsp2/3-positive RTCs (Fig. 5B), indicating that this construct has a dominant negative effect on virus replication. In the very few cases, approximately 4% of the cells expressing GFP-N^{m6m1}, RTCs were present in the same number and had a similar size as in cells expressing GFP-N (not shown), but GFP-N^{m6m1} was not recruited onto RTCs (Fig. 5A and 5C). Altogether these results show that N protein binding to nsp3 is required for its recruitment to the RTCs and possibly also for MHV RNA synthesis and replication.

N protein recruitment to RTCs is crucial for MHV replication.

JVI

To determine whether blocking N protein recruitment to the RTCs leads to a defect in CoV life cycle, we performed a series of experiments to examine whether N^{m6m1} has indeed a dominant negative effect on MHV replication and/or assembly/egression.

We took advantage of the MHV-2aFLS strain, which carries the genes encoding for firefly luciferase and allows assessing virus replication by monitoring the activity of this enzyme (49). We transfected the plasmid expressing GFP, GFP-N or GFP-N^{m6m1} fusion protein into HeLa-CEACAM1a cells for 48 h before exposing them to different multiplicity of infection (MOI) of MHV-2aFLS, *i.e.*, 2.5, 5 and 10, and measuring luciferase activity at 7 h post-infection (p.i.). As shown in Fig. 6A, expression of wild type N protein promoted viral replication exposed to different amounts of virus over time as one would have expected (26-29). Very interestingly, there was a significant decrease in luciferase expression in cells transfected with GFP-N^{m6m1} compared to those expressing GFP-N, but also expressing GFP alone, showing that GFP-N^{m6m1} cannot promote viral replication as the wild type protein, on the contrary, it has a dominant negative effect. Using the same approach, we also explored whether the presence of N^{m6m1} has a permanent negative effect of viral replication or whether it was just retarding it. To this aim, cells transfected with the various constructs were infected with MHV-2aFLS at MOI 5 before measuring luciferase activity 5, 7 and 9 h p.i. (Fig. 6B and not shown). In this experiment as well, the GFP-N chimera stimulated replication over time and at all the examined time points, while GFP-N^{m6m1} had a pronounced inhibitory effect on MHV replication.

To confirm these observations using a wild type MHV strain, we explored the production of viral N protein by western blot at different time points after inoculating the MHV-A59 strain. HeLa-CEACAM1a cells were transfected with the plasmid carrying GFP, GFP-N or GFP-N^{m6m1} for 48 h before to be infected with MHV at MOI for 5 h, 7 h or 9 h (Fig. 6C, 6D and

JVI

not shown). Viral N protein synthesis was again stimulated by the presence of ectopically transfected GFP-N over time but not by GFP-N^{m6m1}. In the same experiment, we also collected the culture supernatants of cells and determined the virus titer to explore whether MHV viral particle production and egression was impaired in cells expressing GFP-N^{m6m1}. This was indeed the case as the virion titer was decreased in cells expressing GFP-N^{m6m1} compared to the ones expressing GFP or GFP-N (Fig. 6E). Altogether these results show that N^{m6m1} has a dominant negative effect on MHV life cycle.

N protein association to nsp3 enhances RTCs-mediated viral RNA synthesis.

The principal role of CoV RTCs is the replication and transcription of the viral RNA. It remains unknown, however, whether the specific N protein recruitment to the RTCs has a regulatory role on viral RNA synthesis, and whether it is influencing gRNA or sgmRNA transcription differently.

To examine the specific relevance of the N protein-nsp3 interaction in the transcription of gRNA and sgmRNA, HeLa-CEACAM1a cells transfected with the plasmid expressing GFP, GFP-N or GFP-N^{m6m1} for 48 h were inoculated with MHV-A59 for 5, 7 and 9 h (Fig. 7A and not shown) before extracting the RNA. The mRNA was quantified by real time (RT)-PCR using sets of primers that allow to specifically assess the synthesis of gRNA and of 4 sgmRNA transcripts (Table 1). Expression of GFP-N stimulated the synthesis of both gRNA and sgmRNA in comparison to cells expressing GFP only, over time and at all the examined time points (Fig. 7A and not shown). In contrast, GFP-N^{m6m1} expression was unable upregulate gRNA and sgmRNA. This result shows that N protein association to RTCs stimulates the replication and transcription activity of these complexes.

JVI

To prove this observation with a different approach, we turned to an *in vitro* viral RNA synthesis (IVRS) assay using a membrane fraction enriched in RTCs, which has recently been devised to study the host factor requirement for the sgmRNA transcription by SARS-CoV RTCs (50). The advantage of *in vitro* assays is that proteins and other components can be easily added, and determine their effect on viral RNA synthesis. First, osmotically lysed MHV-infected cells were centrifuged at 13,000 g to separate dense membranes containing RTCs (P13) from the cytosol (S13). As expected, the ER integral membrane protein VAP-A was entirely found in the P13 pellet while cytoplasmic GAPDH was mainly in the S13 supernatant (Fig. 7B). To confirm the enrichment of RTCs in the P13 fraction, we probed the samples with anti-N antibodies and as expected (50), RTCs were exclusively detected in the P13 fraction. Next, we tested the best experimental conditions to detect RNA synthesis by MHV RTCs *in vitro*. Similar to the protocol established for SARS CoV (50), the P13 fraction from MHV-infected and non-infected cells were mixed with nucleoside triphosphates, an ATP-regeneration system and actinomycin D, a potent inhibitor of host cellular transcription. To assess the synthesis of both sgmRNA and gRNA, we employed quantitative (RT)-PCR instead of labelling using radioactive nucleoside triphosphates (50). The IVRS assays showed that viral RNA was more effectively synthesized when the P13 fraction from MHV-infected cells (P13-MHV) was present in the reaction mixtures (Fig. 7C). Since it was shown that host factors that are present in the S13 supernatant fraction are required for viral RNA synthesis *in vitro* (50), we added either S13 from infected cells and compared the viral RNA synthesis rate with samples not containing S13 (column 2 vs column 3). Interestingly, we did not observe an enhancement of viral RNA synthesis in the presence of S13 from infected cells, indicating that the P13 fraction was sufficient to sustain *in vitro* viral RNA synthesis (Fig. 7C). Subsequently we explored whether adding different amounts

JVI

of N protein to the IVRS assay, enhanced viral transcription. As shown in Fig. 7D, we found that 1 µg of protein extract from N protein-expressing bacteria was providing the maximal stimulation of MHV RTCs-mediated viral RNA synthesis. Lower amounts of the bacterial extracts had a less pronounced effect while higher had an inhibitory impact.

Finally, we carried out the IVRS assay in presence of 1 µg of bacterial extract from *E. coli* expressing equal amounts of N or N^{m6m1} protein. Although wild type N protein was able to enhance viral RNA synthesis as shown in Fig. 7A, addition of N^{m6m1} did not increase the production of viral RNA (Fig. 7E). This result supports the notion that the N interaction with nsp3 stimulates the RNA synthesis activity of MHV RTCs.

JVI

DISCUSSION

A crucial step in CoV life cycle is the synthesis of sgmRNA and gRNA, which principally takes place at the RTCs (14), a complex composed by the nsp proteins that dynamically interacts with N protein (5, 39, 40). In this study, we investigated the relevance of the N protein-RTCs interaction during MHV life cycle. Our Y2H analysis represents the first study that systematically assessed the binding of all MHV nsp proteins with the N protein (Fig. 1B), and corroborates previous studies showing that nsp3 is the main RTCs component interacting with MHV N protein (40, 41, 44, 45). Although, a similar Y2H-based analysis with SARS-CoV proteins failed to uncover binding between nsp3 and N protein (51), we were able to detect an interaction between SARS-CoV N and nsp3 with our Y2H system and confirmed this binding by an *in vitro* pull-down experiment (not shown), emphasising the importance of this interaction for other CoV as well.

Few approaches have shown that nsp3 interacts with the N protein, but the molecular details of the binding between these two proteins remained to be clarified because of inconsistent conclusions. Hurst and colleagues exploited genetic approaches to both identify nsp3 as a binding partner of MHV N protein, and show that the cytoplasmic N-terminal ubiquitin-like domain of nsp3 and the serine and arginine (SR)-rich region of the N2a domain of the N protein, may be important for this interaction (40, 41). They also provided *in vitro* evidence that N protein association with RNA is not relevant for its interaction with the N-terminus of nsp3 (40, 41). An *in solution* study using nuclear magnetic resonance (NMR) and isothermal titration calorimetry, found that the N1b-N2a fragment, but not N1b and N2a individually, binds nsp3 with high affinity (44). Consistent with the other studies, this result indicates that at least one nsp3-binding determinant localizes to the SR-rich region-containing N2a domain of the N

JVI

protein (40, 41). This domain alone, however, is not sufficient to maintain high-affinity binding to nsp3 and this suggests the presence of one or more interaction domains in the N1b-N2a fragment (44). Using *in silico* modelling, it has recently reached the conclusion that two regions in the N1b domain of MHV N protein, comprising the residues Lys113, Arg125, Tyr127 and Glu173 and Tyr190, are involved in N protein-nsp3 association (45). Our detailed examinations of the association between purified nsp3^{N} and different N variants using *in vitro* pull-down experiments, conciliates the previous observations because it demonstrates that indeed both the N1b and N2a interact with nsp3^{N}, with N1b having a stronger binding affinity than N2a (Fig. 2). In particular, we found that when concomitantly mutated, two sets of amino acids in N1b (K101/Y103/W104 and F128/Y129/Y130/T133) and two in N2a (S197/R202/S203/S205A and L240/V241/L242) regions, lead to a defect in the interaction of these domains with nsp3^{N}. Interestingly, single set of mutations in either the N1b or the N2a region, however, did not show a major defect in the association between the N1-N2a fragment and nsp3^{N} (Fig. 3C), indicating a redundancy in binding of the two different protein domains. In agreement with this notion, the combination of mutations in N1b and N2a region completely blocked the interaction between full-length MHV N and nsp3^{N} (Fig. 4A).

What is the relevance of N protein-nsp3 interaction in CoV life cycle? Co-transfection of MHV N protein mRNA and gRNA leads to a significant increase in infectivity compared to the transfection with gRNA alone (41). A similar beneficial role of N protein for infection has been shown for other CoV as well (26, 27). Despite these observations, the mechanism how CoV N proteins stimulate CoV infections has remained unknown. To the best of our knowledge, our data are the first to reveal that the direct association of N protein with RTCs is a critical step for MHV infection because the impairment of this interaction has a negative effect on MHV replication and progeny production (Fig. 5 and 6). This notion is also indirectly sustained by the fact that it was not possible to generate MHV mutant strains expressing N^{m6m1} using two distinct approaches. In particular, we found that N^{m6m1} expression in host cells has a dominant negative effect on MHV life cycle. Our interpretation of this result is that ectopically expressed N^{m6m1} outcompetes the virus-encoded N protein, especially early during infection when the first RTCs are formed. This leads to the formation of N protein oligomers that are principally composed by N^{m6m1} and therefore unable to be effectively recruited to RTCs. We furthermore show that wild type N protein which is correctly recruited to RTCs promotes local viral RNA synthesis, *i.e.*, gRNA replication and sgmRNA transcription, *in vivo* and *in vitro* (Fig. 7 and not shown). In contrast, the nsp3-binding mutant N^{m6m1} is not able to do so. This finding reveals that N protein recruitment and association to RTCs is critical for the optimal function of these complexes in viral RNA synthesis and ultimately infection.

Interestingly, the $N2a^{m2}$ variant that affects the phosphorylation site modified cellular GSK-3 that enables the transition from discontinuous transcription of sgmRNA to continuous synthesis of longer sgmRNA and gRNA (32), affects the binding of this fragment to nsp3 but not that of the entire N protein (Fig. 4A). As a result, a speculative idea is that phosphorylation of the SR-rich region, which is part of the N2a domain, triggers the recruitment of the RNA helicase DDX1 (32) but also abrogates one of the interactions between the N protein and nsp3. This latter event could help to accommodate the RNA helicase DDX1 in the N protein-RTCs complexes and/or promote the transition in the transcription mode by influencing the ultrastructural organization of the N protein-RTCs complexes.

Altogether, our findings support a model where the N protein recruitment to RTCs via nsp3 binding, stimulates the synthesis of viral RNA. It remains unclear, however, how and why

JVI

the N protein orchestrates viral RNA synthesis. A speculative idea is that the N protein-nsp3 interaction induces enzymatic activities and/or provides a more structured conformation of the complexes that positively influences protein and RNA interactions at the RTCs. This could guarantee the sufficient production of structural proteins necessary to efficiently encapsulate the newly formed ribonucleoprotein complexes into virions. Our current working model is that N proteins probably oligomerize in the cytosol and then are recruited to RTCs, which are present at the DMVs and convoluted membranes, through the binding to nsp3 (Fig. 8). At the RTCs, the N oligomers stimulate viral RNA synthesis. While local production of gRNA and presence of N oligomers may promote the formation of ribonucleoprotein complexes, newly transcribed sgmRNA would guarantee sufficient synthesis of structural proteins. In contrast, N^{m6m1}-containing oligomers cannot be efficiently recruited to the RTCs and viral RNA synthesis fails to be stimulated (Fig. 8), resulting in a strongly impaired CoV infection.

Further investigations are needed to unveil how N protein binding to RTCs mechanistically enhances viral RNA synthesis. Nonetheless, our findings already pave the way for future studies aimed at developing novel therapies against CoV that specifically target the interaction between N proteins and nsp3. In particular, purified N protein and $nsp3^{N}$ could be exploited in screening for drug compounds that affect their binding using systems like the Biacore^{TM}.

JVI

MATERIALS AND METHODS

Cell culture and virus. LR7 (52) and HeLa-CEACAM1a cells (48) were maintained in Dulbecco's Modified Eagle Medium (DMEM; Cambrex Bioscience, Walkersville, MD) supplemented with 10% fetal calf serum (Bodinco Alkmaar, The Netherlands), 100 IU of penicillin/ml and 100 µg/ml of streptomycin (both from Life Technologies, Rochester, NY). HeLa-CEACAM1a cells were cultured in presence of 800 µg/ml geneticin G-418 sulphate (G418; Gibco, Waltham, MA). Wild type MHV-A59 was propagated in LR7 cells in DMEM. The MHV strain carrying luciferase used in our study was MHV-2aFLS (49). Virus titers of the culture supernatants were determined with a diluted factor of three on LR7 cells and the culture infectious dose ($TCID_{50}$) units per ml of supernatant were calculated according to the Reed-Muench method (53). $TCID_{50}$/ml values were then converted into PFU/µl using the following equations: $TCID_{50}$/ml × 0.00069 (54).

Plasmids. The pGBDU plasmids carrying the 16 MHV nsp proteins and the pGAD vectors expressing the MHV N protein or its truncated variants, were generated by PCR of MHV cDNA using appropriate primers and subsequent cloning into the pGAD-C1 and pGBDU-C1 vector, respectively (42). The sequences coding for either full-length MHV N protein or its truncations, *i.e.*, N1 (amino acids 1 to 194), N2a (amino acids 195 to 257) and N2b-N3 (amino acids 258 to 454), were amplified by PCR from MHV cDNA and cloned into pET32c (EMD Millipore, Amsterdam, The Netherlands) vector using *Bam*HI and *Xho*I, creating the pET32c-N, pET32C-N1, pET32C-N2a and pET32C-N2b-N3 plasmids, which express the 6×His-N, 6×His-N1, 6×His-N2a and 6×His-N2b-N3 fusion protein, respectively. The sequences coding for MHV $nsp3^N$ was amplified by PCR from MHV cDNA and cloned into the pGEX vector (GE Healthcare, Little Chalfont, United Kingdom) using *Bam*HI and *Xho*I, creating the pGEX-$nsp3^N$

JVI

construct, which expresses the GST-nsp3^{N} chimera. The mutated N proteins were created by PCR from pET32c-N construct, generating the pET32c-N2a^{m1} (amino acids 195 to 257 carrying the L240E, V241E and L242E mutations), pET32c-N2a^{m2} (amino acids 195 to 257 carrying the S197A, R202A, S203A and S205A mutations), pET32c-N1^{m3} (amino acids 1 to 194 carrying the T73A, Q74A and K77A mutations), pET32c-N1^{m4} (amino acids 1 to 194 carrying with K101A, Y103A and W104A mutations), pET32c-N1^{m5} (amino acids 1 to 194 carrying the R109A, R110A and K113A mutations), pET32c-N1^{m6} (amino acids 1 to 194 carrying the F128A, Y129A, Y130A and T133A mutations), pET32c-N^{m4m1} (amino acids 1 to 454 carrying the L240E, V241E, L242E, K101A, Y103A and W104A mutations), pET32c-N^{m6m1} (amino acids 1 to 454 carrying the L240E, V241E, L242E, F128A, Y129A, Y130A and T133A mutations), pET32c-N^{m4m2} (amino acids 1 to 454 carrying the S197A, R202A, S203A and S205A, K101A, Y103A and W104A mutations), and pET32c-N^{m6m2} (amino acids 1 to 454 carrying the S197A, R202A, S203A and S205A, F128A, Y129A, Y130A and T133A mutations) plasmids (Fig. 1A and 3A). To express mCherry tagged version of the different N protein mutants in cells, the GFP coding sequence was replaced in the pcDNA5-GFP vector with the one of mCherry using *Str*I and *BsrG*I to create pcDNA5-mCherry. PCR-generated *N*, N^{m4m1}, N^{m6m1}, N^{m4m2} and N^{m6m2} sequences were subsequently inserted as *Hind*III- *Bam*HI fragments into pcDNA5-mCherry generating pcDNA5-mCherry-N, pcDNA5-mCherry-N^{m4m1}, pcDNA5-mCherry-N^{m6m1}, pcDNA5-mCherry-N^{m4m2} and pcDNA5-mCherry-N^{m6m2}. To express GFP-tagged version of the mutant N proteins in cells, GFP was cloned into the pcDNA3.1 vector as a *Xho*I-*Bam*HI fragment creating pcDNA3.1-GFP. PCR-generated N, N^{m4m1}, N^{m6m1}, N^{m4m2} and N^{m6m2} were subsequently inserted as *Bam*HI-*Hind*III fragments into pcDNA3.1-GFP generating pcDNA3.1-GFP-N, pcDNA3.1-GFP-N^{m4m1},

JVI

pcDNA3.1-GFP-N^{m6m1}, pcDNA3.1-GFP-N^{m4m2} and pcDNA3.1-GFP-N^{m6m2}. All point mutations were verified by DNA sequencing.

Bacterial extracts. *Escherichia coli* BL-21 carrying plasmid expressing the various GST- or 6×His-tagged fusion proteins, were grown in 125 ml of LB medium (0.5% yeast extract, 1% tryptone, 1% NaCl) to a late exponential phase. After inducing protein expression by addition of 0.5 mM isopropyl-β-D-thiogalactopyranoside, cells were grown at 37˚C or 20˚C for 4 h or 16 h. Bacteria were harvested, resuspended in 4 ml of lysis buffer [PBS (137 mM NaCl, 10 mM phosphate, pH of 7.4, 2.7 mM KCl), 5 mM DTT, 1 mg/ml lysozyme, 1 mM PMSF, 10% glycerol, 1% Triton X-100 and complete protease inhibitor (Roche, Basel Switzerland)] and lysed by two sonication rounds of 10 s using a Branson sonicator (Danbury, Connecticut, United States). The bacterial lysates were cleared by centrifugation at 13,000 rpm for 10 min at 4˚C. The concentration of 6×His-tagged proteins was measured using the BCA kit (Promega, Madison, WI). Proteins were not further purified and bacterial lysates were stored at -80˚C until use.

For purification of GST fusion proteins, lysates were incubated with 125 µl of GSH-sepharose (GE Healthcare, Little Chalfont, United Kingdom), which had been pre-washed in PBS on a rotatory wheel at 4˚C for 2 h.

Cell extracts. For the preparation of cell extracts, LR7 cells were grown in 10 cm dishes before to be either mock-treated or inoculated with MHV at a MOI of 1. After 8 h, cells were lysed by a 5 min sonication in 1.2 ml of lysis buffer and supernatants were cleared by centrifugation at 13,000 rpm for 10 min at 4˚C. RNase A (Invitrogen, Carlsbad, CA) treatments were carried out by incubating 200 µl of cell extracts with 2.5 U of enzyme on ice for 30 min, immediately prior to pull-downs.

JVI

Yeast two-hybrid assay. The *Saccharomyces cerevisiae* test strain PJ69 (*MAT*a *trpl-901 leu2-3,112 ura3-52 his3-200 gal4*Δ *gal80Δ LYS2*::*GALl-HIS3 GAL2-ADE2 met2*::*GAL7-lacZ*) was used for the assay (42). The prey (AD) and bait (BD) vectors were co-transformed into the PJ69 strain using lithium acetate. Co-transformed colonies were selected on synthetic minimal medium (SMD; 0.67% yeast nitrogen base without amino acids, 2% glucose, and auxotrophic amino acids as needed) lacking uracil and leucine before spotting them on SMD medium lacking uracil, leucine and histidine to determine whether the tested proteins interact. The combination of empty pGAD and pGBDU vectors was used as negative growth control (42), while the one of pGAD-Atg19 and pGBDU-Atg11 was the control for a positive interaction (55).

Pull-down experiments. For the pull-down experiments, GSH-sepharose bound GST fusion proteins were incubated with 200 µl of bacterial extract or 200 µl of LR7 cell extract on a rotatory wheel at 4˚C for 2 h, and subsequently washed three times in PBS supplemented with 5 mM DTT, 10% glycerol, 1% Triton X-100 and one time in PBS buffer at 4˚C. Proteins bound to the sepharose beads were eluted in 20 µl of sample buffer (65.8 mM Tris-HCl, pH6.8, 26.3% glycerol, 2.1% SDS and 0.01% bromophenol blue) by boiling and then subjected to SDS-PAGE, blotted onto PVDF membranes and visualized by either membrane staining with Ponceau Red or western blot analysis using an anti-6×His monoclonal antibody (HIS H8, Thermofisher, Waltham, MA) or an anti-N protein monoclonal antibody (a kind gift of Stuart Siddell, University of Bristol, (56)). Bound primary antibodies were detected using the Alexa-680-conjugated goat polyclonal anti-mouse IgG antibody (Life Technologies) and signals visualized with an Odyssey imaging system (LI-COR, Lincoln, NE).

Subcellular fractionation and glycerol gradient sedimentation. Bacterial extracts (Ext) from *E. coli* expressing 6×His-tagged N, N^{m4m1}, N^{m6m1}, N^{m4m2} or N^{m6m2} fusion proteins,

JVI

were loaded on the top of a 2.2 ml continuous 15-40% glycerol gradient in lysis buffer (w/v) prepared using the Gradient Master machine (Biocomp, New Brunswick, Canada). After centrifugation at 135,000 × *g* for 75 min at 4˚C in a TLS55 rotor (Beckman Coulter, Brea, CA), 11 fractions of 200 µl were collected from the top to the bottom of the gradient. After precipitation by addition of 20 µl of tri-chloroacetic acid (final concentration: 10%), proteins were resolved by SDS-PAGE and analyzed by western blot using monoclonal antibodies against the MHV N protein.

Immuno-fluorescence analyses. HeLa-CEACAM1a or LR7 cells were grown on 12-mm cover slips, transfected and infected before being fixed with 4% paraformaldehyde at the indicated p.i. times. After permeabilization using 0.2% Triton X-100 and subsequent blocking with PBS buffer containing 1% FCS, viral non-structural protein2/3 were detected using the anti-nsp2/nsp3 antiserum, a kind gift of Susan Baker (57), followed by incubation with secondary antibody conjugated to either Alexa-488 or Alexa-568 (Life Technologies). Fluorescence signals were captured with a Leica sp8 confocal microscope (Leica, Wetzlar, Germany).

Luciferase assay. HeLa-CEACAM1a cells transfected in 96-well plates were infected with the MHV-2aFLS strain at the indicated MOI and for the indicated times, before to be washed with PBS and incubated with 50 µl of Lysis buffer (Firefly Luciferase Flash Assay kit, Thermofisher), at room temperature for 15 min before storing the cell lysates at -20˚C. Subsequently, 25 µl aliquots of thawed cell lysates were used to assess firefly luciferase expression using the Firefly luciferase flash assay kit (58). Enzymatic activities were measured with a GloMax-Multi Detection System (Promega) and the following program: 25 µl substrate; 2 s delay; 10 s measurements. Background luminescence was subtracted from each obtained value and the results were normalized towards infected cells transfected with an empty vector exclusively expressing GFP.

Western blot analyses. HeLa-CEACAM1a cells grown in 6-well plates were infected with the MHV-A59 strain at MOI 5 for the indicated times, before to be washed with cold PBS and harvested in 100 µl of 2× sample buffer on ice for 30 min, sonicated for 1 min and boiled. Equal protein amounts were separated by SDS-PAGE and after western blot, proteins were detected using specific antibodies against MHV N protein, GFP (Roche) and β-actin (Merck Millipore, Burlington, MA), and the Odyssey imaging system. Protein signal intensities were normalized and quantified using the ImageJ software (NIH, Bethesda, MD).

RNA isolation, cDNA synthesis and RT-PCR. HeLa-CEACAM1a cells grown in 96-well plates were washed with ice-cold PBS and lysed with 30 µl of lysis buffer containing DNase I at room temperature for 5 min before adding 3 ul of Stop solution for 3 min at room temperature according to the manufacturer's protocol (Power SYBR Green Cells-to-CT kit, Thermofisher). Reverse transcription of the mRNA using a polyT primer, cDNA synthesis and quantitative PCR were performed in a CFX connect Thermocycler (Bio-Rad, Berkeley, CA). Used primers are described in Table 1. The levels of gRNA and the analysed sgmRNA were normalized to that of GAPDH according to the comparative cycle threshold method used for quantification as recommended by the manufacture's protocol.

IVRS assay. MHV- or mock-infected LR7 cells grown on 5 different 15 cm dishes (approximately 1.5×10^7 cells/dish) were harvested by trypsinization at 8 h p.i. To inhibit cellular transcription, 2 µg/ml of actinomycin D (Sigma, Saint Louis, MO) were present in all solutions used for harvesting and washing of the cells. After washing with PBS, cells were resuspended in 2 ml ice-cold hypotonic buffer (20 mM HEPES, pH 7.4, 10 mM KCl, 1.5 mM $MgOAc_2$, 1 mM

Journal of Virology JVI Journal of Virology

JVI

DTT, 133 U/ml RNase A inhibitor (Promega)) and incubated at 4˚C for 10 min. Cells were disrupted using a Dounce homogenizer by giving 30 strokes with a tight-fitting pestle. Isotonic conditions were restored by adding HEPES, sucrose, and DTT, which resulted in a final lysate containing 35 mM HEPES, pH 7.4, 250 mM sucrose, 8 mM KCl, 2.5 mM DTT, 1 mM $MgOAc_2$, 2 µg/ml actinomycin D and 130 U/ml RNase A inhibitor. Nuclei, large debris and any remaining intact cells were removed by two successive centrifugations at 1,000×g for 5 min, and the resulting post-nuclear supernatant (PNS) was either assayed immediately for RTCs activity or stored at -80˚C. A 13,000×g pellet (P13) and supernatant (S13) fraction were prepared from PNS by centrifugation at 13,000×g for 10 min at 4˚C. The P13 pellet was resuspended in the dilution buffer (35 mM HEPES, pH 7.4, 250 mM sucrose, 8 mM KCl, 2.5 mM DTT, 1 mM $MgOAc_2$, 2 µg/ml actinomycin D, and 130 U/ml RNase A inhibitor), in 1/9 of the original PNS volume from which the pellet had been prepared.

IVRS assay mixtures were prepared by mixing 15 µl of P13 and 30 µl of S13, supplemented with or without different amounts of bacterial extracts from *E. coli* expressing 6×His-N or 6×His-N^{m6m1}. Identical level of expression of these two fusion proteins in bacterial extracts used for the IRVS assays were verified by western blot using an anti-6×His monoclonal antibody. Pure proteins could not be used because unstable and therefore were getting partially degraded during the purification procedure. The total volume of each mixture was adjusted to 75 µl with dilution buffer and two 25 µl aliquots were made from this mixture. 5.6 ul of 100 mM creatine phosphate (Sigma, final concentration 20 mM), and 0.28 ul of 1000 U/ml creatine phosphokinase (Sigma, final concentration 10 U/ml) to both of these aliquots. The IVRS assay was initiated in one of these aliquots (reaction sample) by addition of nucleoside triphosphate (final concentrations: 1 mM ATP, 0.25 mM GTP, 0.25 mM UTP and 0.18 mM CTP). The

JVI

second aliquot served as a control (background sample) and dilution buffer was added instead of the nucleoside triphosphates. The IVRS assays were carried out at 30˚C for 100 min before to be stopped by addition first of 30 µl of lysis buffer containing DNase I at room temperature for 5 min and then of 3 µl of Stop solution for 3 min at the same temperature (both solutions from the Power SYBR Green Cells-to-CT kit, Thermofisher). Reverse transcription of the RNA, cDNA synthesis and quantitative PCR were performed in a CFX connect Thermocycler using appropriate primers. The expression levels of the S gene, which is part of the viral RNA (both sgmRNA and gRNA), were normalized to that of GAPDH in each sample, according to the comparative cycle threshold method used for quantification as recommended by the manufacture's protocol. Finally, the value of each background sample was subtracted to the value of the corresponding reaction sample to determine the difference due to S gene *in vitro* synthesis.

Statistical analysis. Statistical significance was evaluated using the two-tailed heteroscedastic *t*-test before calculating the *p*-values. Individual data points from each independent experiment were used for the calculation of the significance. The number of independent experiments is indicated in each figure legend.

ACKNOWLEDGEMENTS

We thank Susan Baker (Loyola University Chicago, Unites States of America) and Stuart Siddell (University of Bristol, United Kingdom) for antibodies, and Anke Huckriede (University of Groningen, The Netherlands) for critical reading of the manuscript. This work was supported by SNF Sinergia (CRSII3_154421) and ZonMW VICI (016.130.606) grants (to Fulvio Reggiori). Y.C. was supported by a Chinese Scholarship Council PhD fellowship (CSC No.

JVI

201406610008). The funders had no role in study design, data collection and interpretation, or the decision to submit the work for publication.

JVI

REFERENCES

1. **Cui J, Li F, Shi ZL.** 2019. Origin and evolution of pathogenic coronaviruses. Nat Rev Microbiol **17:**181-192.

2. **Perlman S, Netland J.** 2009. Coronaviruses post-SARS: update on replication and pathogenesis. Nat Rev Microbiol **7:**439-a50.

3. **Fehr AR, Perlman S.** 2015. Coronaviruses: an overview of their replication and pathogenesis. Methods Mol Biol **1282:**1-23.

4. **Woo PC, Lau SK, Lam CS, Lau CC, Tsang AK, Lau JH, Bai R, Teng JL, Tsang CC, Wang M, Zheng BJ, Chan KH, Yuen KY.** 2012. Discovery of seven novel mammalian and avian coronaviruses in the genus deltacoronavirus supports bat coronaviruses as the gene source of alphacoronavirus and betacoronavirus and avian coronaviruses as the gene source of gammacoronavirus and deltacoronavirus. J Virol **86:**3995-4008.

5. **Sawicki SG, Sawicki DL, Siddell SG.** 2007. A contemporary view of coronavirus transcription. J Virol **81:**20-29.

6. **Brockway SM, Clay CT, Lu XT, Denison MR.** 2003. Characterization of the expression, intracellular localization, and replication complex association of the putative mouse hepatitis virus RNA-dependent RNA polymerase. J Virol **77:**10515-10527.

7. **Snijder EJ, van der Meer Y, Zevenhoven-Dobbe J, Onderwater JJ, van der Meulen J, Koerten HK, Mommaas AM.** 2006. Ultrastructure and origin of membrane vesicles associated with the severe acute respiratory syndrome coronavirus replication complex. J Virol **80:**5927-5940.

8. **Hagemeijer MC, Rottier PJ, de Haan CA.** 2012. Biogenesis and dynamics of the coronavirus replicative structures. Viruses **4:**3245-3269.

JVI

9. **V'Kovski P, Gerber M, Kelly J, Pfaender S, Ebert N, Braga Lagache S, Simillion C, Portmann J, Stalder H, Gaschen V, Bruggmann R, Stoffel MH, Heller M, Dijkman R, Thiel V.** 2019. Determination of host proteins composing the microenvironment of coronavirus replicase complexes by proximity-labeling. Elife. **8** (doi: 10.7554/eLife.42037).

10. **Knoops K, Kikkert M, Worm SH, Zevenhoven-Dobbe JC, van der Meer Y, Koster AJ, Mommaas AM, Snijder EJ.** 2008. SARS-coronavirus replication is supported by a reticulovesicular network of modified endoplasmic reticulum. PLoS Biol **6:**e226.

11. **Gosert R, Kanjanahaluethai A, Egger D, Bienz K, Baker SC**. 2002. RNA replication of mouse hepatitis virus takes place at double-membrane vesicles. J Virol **76:**3697-3708.

12. **Ulasli M, Verheije MH, de Haan CA, Reggiori F.** 2010. Qualitative and quantitative ultrastructural analysis of the membrane rearrangements induced by coronavirus. Cell Microbiol **12:**844-861.

13. **Krupovic M, Koonin EV.** 2017. Multiple origins of viral capsid proteins from cellular ancestors. Proc Natl Acad Sci U S A **114:**E2401-E2410.

14. **McBride R, van Zyl M, Fielding BC.** 2014. The coronavirus nucleocapsid is a multifunctional protein. Viruses **6:**2991-3018.

15. **Saikatendu KS, Joseph JS, Subramanian V, Neuman BW, Buchmeier MJ, Stevens RC, Kuhn P.** 2007. Ribonucleocapsid formation of severe acute respiratory syndrome coronavirus through molecular action of the N-terminal domain of N protein. J Virol **81:**3913-3921.

16. **Fan H, Ooi A, Tan YW, Wang S, Fang S, Liu DX, Lescar J.** 2005. The nucleocapsid protein of coronavirus infectious bronchitis virus: crystal structure of its N-terminal domain and multimerization properties. Structure **13:**1859-1868.

JVI

17. **Jayaram H, Fan H, Bowman BR, Ooi A, Jayaram J, Collisson EW, Lescar J, Prasad BV.** 2006. X-ray structures of the N- and C-terminal domains of a coronavirus nucleocapsid protein: implications for nucleocapsid formation. J Virol **80:**6612-6620.

18. **Grossoehme NE, Li L, Keane SC, Liu P, Dann CE, 3rd, Leibowitz JL, Giedroc DP.** 2009. Coronavirus N protein N-terminal domain (NTD) specifically binds the transcriptional regulatory sequence (TRS) and melts TRS-cTRS RNA duplexes. J Mol Biol **394:**544-557.

19. **Lo YS, Lin SY, Wang SM, Wang CT, Chiu YL, Huang TH, Hou MH.** 2013. Oligomerization of the carboxyl terminal domain of the human coronavirus 229E nucleocapsid protein. FEBS Lett **587:**120-127.

20. **Chang CK, Sue SC, Yu TH, Hsieh CM, Tsai CK, Chiang YC, Lee SJ, Hsiao HH, Wu WJ, Chang WL, Lin CH, Huang TH.** 2006. Modular organization of SARS coronavirus nucleocapsid protein. J Biomed Sci **13:**59-72.

21. **Chen CY, Chang CK, Chang YW, Sue SC, Bai HI, Riang L, Hsiao CD, Huang TH.** 2007. Structure of the SARS coronavirus nucleocapsid protein RNA-binding dimerization domain suggests a mechanism for helical packaging of viral RNA. J Mol Biol **368:**1075-1086.

22. **Gui M, Liu X, Guo D, Zhang Z, Yin CC, Chen Y, Xiang Y.** 2017. Electron microscopy studies of the coronavirus ribonucleoprotein complex. Protein Cell **8:**219-224.

23. **Cong Y, Kriegenburg F, de Haan CAM, Reggiori F.** 2017. Coronavirus nucleocapsid proteins assemble constitutively in high molecular oligomers. Sci Rep **7:**5740.

24. **Ma Y, Tong X, Xu X, Li X, Lou Z, Rao Z.** 2010. Structures of the N- and C-terminal domains of MHV-A59 nucleocapsid protein corroborate a conserved RNA-protein binding mechanism in coronavirus. Protein Cell **1:**688-697.

25. **Kuo L, Hurst-Hess KR, Koetzner CA, Masters PS.** 2016. Analyses of coronavirus assembly interactions with interspecies membrane and nucleocapsid protein chimeras. J Virol **90:**4357-4368.

26. **Almazan F, Galan C, Enjuanes L.** 2004. The nucleoprotein is required for efficient coronavirus genome replication. J Virol **78:**12683-12688.

27. **Schelle B, Karl N, Ludewig B, Siddell SG, Thiel V.** 2005. Selective replication of coronavirus genomes that express nucleocapsid protein. J Virol **79:**6620-6630.

28. **Thiel V, Herold J, Schelle B, Siddell SG.** 2001. Viral replicase gene products suffice for coronavirus discontinuous transcription. J Virol **75:**6676-6681.

29. **Zuniga S, Cruz JL, Sola I, Mateos-Gomez PA, Palacio L, Enjuanes L.** 2010. Coronavirus nucleocapsid protein facilitates template switching and is required for efficient transcription. J Virol **84:**2169-2175.

30. **Chen H, Gill A, Dove BK, Emmett SR, Kemp CF, Ritchie MA, Dee M, Hiscox JA.** 2005. Mass spectroscopic characterization of the coronavirus infectious bronchitis virus nucleoprotein and elucidation of the role of phosphorylation in RNA binding by using surface plasmon resonance. J Virol **79:**1164-1179.

31. **Spencer KA, Dee M, Britton P, Hiscox JA.** 2008. Role of phosphorylation clusters in the biology of the coronavirus infectious bronchitis virus nucleocapsid protein. Virology **370:**373-381.

32. **Wu CH, Yeh SH, Tsay YG, Shieh YH, Kao CL, Chen YS, Wang SH, Kuo TJ, Chen DS, Chen PJ.** 2009. Glycogen synthase kinase-3 regulates the phosphorylation of severe acute respiratory syndrome coronavirus nucleocapsid protein and viral replication. J Biol Chem **284:**5229-5239.

JVI

33. **Peng TY, Lee KR, Tarn WY.** 2008. Phosphorylation of the arginine/serine dipeptide-rich motif of the severe acute respiratory syndrome coronavirus nucleocapsid protein modulates its multimerization, translation inhibitory activity and cellular localization. FEBS J **275:**4152-4163.

34. **Denison MR, Spaan WJ, van der Meer Y, Gibson CA, Sims AC, Prentice E, Lu XT.** 1999. The putative helicase of the coronavirus mouse hepatitis virus is processed from the replicase gene polyprotein and localizes in complexes that are active in viral RNA synthesis. J Virol **73:**6862-6871.

35. **van der Meer Y, Snijder EJ, Dobbe JC, Schleich S, Denison MR, Spaan WJ, Locker JK.** 1999. Localization of mouse hepatitis virus nonstructural proteins and RNA synthesis indicates a role for late endosomes in viral replication. J Virol **73:**7641-7657.

36. **Sims AC, Ostermann J, Denison MR.** 2000. Mouse hepatitis virus replicase proteins associate with two distinct populations of intracellular membranes. J Virol **74:**5647-5654.

37. **Stertz S, Reichelt M, Spiegel M, Kuri T, Martinez-Sobrido L, Garcia-Sastre A, Weber F, Kochs G.** 2007. The intracellular sites of early replication and budding of SARS-coronavirus. Virology **361:**304-315.

38. H**agemeijer MC, Verheije MH, Ulasli M, Shaltiel IA, de Vries LA, Reggiori F, Rottier PJ, de Haan CA.** 2010. Dynamics of coronavirus replication-transcription complexes. J Virol **84:**2134-2149.

39. **Verheije MH, Hagemeijer MC, Ulasli M, Reggiori F, Rottier PJ, Masters PS, de Haan CA.** 2010. The coronavirus nucleocapsid protein is dynamically associated with the replication-transcription complexes. J Virol **84:**11575-11579.

JVI

40. **Hurst KR, Koetzner CA, Masters PS.** 2013. Characterization of a critical interaction between the coronavirus nucleocapsid protein and nonstructural protein 3 of the viral replicase-transcriptase complex. J Virol **87:**9159-9172.

41. **Hurst KR, Ye R, Goebel SJ, Jayaraman P, Masters PS.** 2010. An interaction between the nucleocapsid protein and a component of the replicase-transcriptase complex is crucial for the infectivity of coronavirus genomic RNA. J Virol **84:**10276-10288.

42. **James P, Halladay J, Craig EA.** 1996. Genomic libraries and a host strain designed for highly efficient two-hybrid selection in yeast. Genetics **144:**1425-1436.

43. **Angelini MM, Akhlaghpour M, Neuman BW, Buchmeier MJ.** 2013. Severe acute respiratory syndrome coronavirus nonstructural proteins 3, 4, and 6 induce double-membrane vesicles. MBio. **4:**e00524-13.

44. **Keane SC, Giedroc DP.** 2013. Solution structure of mouse hepatitis virus (MHV) nsp3a and determinants of the interaction with MHV nucleocapsid (N) protein. J Virol **87:**3502-3515.

45. **Tatar G, Tok TT.** 2016. Clarification of interaction mechanism of mouse hepatitis virus (MHV) N and nsp3 protein with homology modeling and protein-protein docking analysis. Curr Comput Aided Drug Des **12:**98-106.

46. **Wu CH, Chen PJ, Yeh SH.** 2014. Nucleocapsid phosphorylation and RNA helicase DDX1 recruitment enables coronavirus transition from discontinuous to continuous transcription. Cell Host Microbe **16:**462-472.

47. **Eriksson KK, Makia D, Thiel V.** 2008. Generation of recombinant coronaviruses using vaccinia virus as the cloning vector and stable cell lines containing coronaviral replicon RNAs. Methods Mol Biol **454:**237-254.

JVI

48. **Verheije MH, Raaben M, Mari M, Te Lintelo EG, Reggiori F, van Kuppeveld FJ, Rottier PJ, de Haan CA.** 2008. Mouse hepatitis coronavirus RNA replication depends on GBF1-mediated ARF1 activation. PLoS Pathog **4:**e1000088.

49. **de Haan CA, van Genne L, Stoop JN, Volders H, Rottier PJ.** 2003. Coronaviruses as vectors: position dependence of foreign gene expression. J Virol 77:11312-23.

50. **van Hemert MJ, van den Worm SH, Knoops K, Mommaas AM, Gorbalenya AE, Snijder EJ.** 2008. SARS-coronavirus replication/transcription complexes are membrane-protected and need a host factor for activity in vitro. PLoS Pathog **4:**e1000054.

51. **von Brunn A, Teepe C, Simpson JC, Pepperkok R, Friedel CC, Zimmer R, Roberts R, Baric R, Haas J.** 2007. Analysis of intraviral protein-protein interactions of the SARS coronavirus ORFeome. PLoS One **2:**e459.

52. **de Haan CA, Masters PS, Shen X, Weiss S, Rottier PJ.** 2002. The group-specific murine coronavirus genes are not essential, but their deletion, by reverse genetics, is attenuating in the natural host. Virology **296:**177-189.

53. **Reed LJ, Muench H.** 1938. A simple method of estimating fifty per cent endpoints . Am J Epidemiol **27:**493-497.

54. **Emery VC.** 1992. Baculovirus expression vectors : choice of expression vector. Methods Mol Biol **8:**287-307.

55. **Yorimitsu T, Klionsky DJ.** 2005. Atg11 links cargo to the vesicle-forming machinery in the cytoplasm to vacuole targeting pathway. Mol Biol Cell **16:**1593-1605.

56. **Schwarz B, Routledge E, Siddell SG.** 1990. Murine coronavirus nonstructural protein ns2 is not essential for virus replication in transformed cells. J Virol **64:**4784-4791.

57. **Schiller JJ, Kanjanahaluethai A, Baker SC.** 1998. Processing of the coronavirus MHV-JHM polymerase polyprotein: identification of precursors and proteolytic products spanning 400 kilodaltons of ORF1a. Virology **242:**288-302.

58. **de Haan CA, Li Z, te Lintelo E, Bosch BJ, Haijema BJ, Rottier PJ.** 2005. Murine coronavirus with an extended host range uses heparan sulfate as an entry receptor. J Virol **79:**14451-14456.

JVI

FIGURE LEGENDS

Figure 1. MHV N protein directly binds to nsp3. (A) Schematic structural organization of MHV N protein and overview of the truncations generated in this study. (B) Y2H assay-based analysis of the interaction between the N protein and each one of the MHV nsp proteins. The plasmid expressing the AD-N fusion protein was co-transformed with the plasmids carrying the nsp gene N-terminally tagged with the BD domain into the Y2H test strain. Transformed cells were selected on a selective medium containing histidine (+His) while the interaction between the two tested proteins was assessed in a selective medium lacking histidine (-His) (42). Growth on -His plates showed that the N protein interacts only with nsp3. (C) Cell extracts from MHV-infected LR7 cells were incubated with RNase A or RNase A mixed with the RNase A inhibitor, or left untreated on ice for 30 min, before being subjected to pull-down with immobilized GST or GST-nsp3^N. Bound proteins were eluted by boiling in sample buffer and analyzed by western blot using an anti-N antibody. Staining of the membrane with Ponceau Red was used to reveal the amount of immobilized GST and GST-nsp3^N. (D) Bacterial lysates from *E. coli* expressing the 6×His-N fusion protein were prepared as described under Material and Methods and incubated with immobilized GST or GST-nsp3^N. Bound proteins were eluted by boiling in sample buffer and examined by western blot using an anti-His antibody. Amounts of immobilized GST and GST-nsp3^N were visualized as in panel C.

Figure 2. Two regions in the MHV N protein are required for its interaction with nsp3. (A) The interaction between nsp3^N and different C-terminal truncations of N protein was tested by Y2H assay as described in Fig. 1B. (B) Bacterial extracts from *E. coli* expressing the 6×His-

JVI

tagged N, N1, N2a or N2b-N3 truncations were incubated with immobilized GST or GST-nsp3^{N}. Isolated proteins were eluted by boiling in sample buffer and analyzed by western blot using the anti-6×His monoclonal antibody. GST and GST-nsp3^{N} were visualized as in Fig. 1C. The symbol * indicates a degradation product of 6×His-N. (C) A bacterial extract from *E. coli* expressing the 6×His-tagged N2a was incubated with immobilized GST or GST-nsp3^{N}. Isolated proteins were eluted and examined as in panel B but western blot membranes but exposure time to visualize the bands was increased 5 times.

Figure 3. Two distinct amino acid stretches mediate N protein interaction with nsp3. (A) *Top part*. The alignment of part of beta-CoV N protein sequences was done using the Jalview software (http://www.jalview.org/download.html). Conserved amino acid were localized on the 3D structure of the N1-N2a domain (24) using the PyMOL software (Schrödinger, New York, NY) to determine which ones are on the surface and thus available for interaction. The amino acids changed in the different mutant variants are indicated with an asterisk and coloured in red. The Ser205 of MHV N protein, which represents the priming site essential for SR-rich region phosphorylation by host cell GSK3, is coloured in violet (32, 46). *Bottom part*. Schematic distribution of the different mutations introduced in the N protein. (B) Bacterial extracts from *E. coli* expressing the 6×His-tagged N1, N1^{m3}, N1^{m4}, N1^{m5}, N1^{m6}, N2a, N2a^{m1} or N2a^{m2} were incubated with immobilized GST or GST-nsp3^{N}. Isolated proteins were eluted by boiling in sample buffer and analyzed by western blot using the anti-6×His monoclonal antibody. GST and GST-nsp3^{N} were visualized as in Fig. 1C. (C) Bacterial extracts from *E. coli* expressing the 6×His-tagged N1-N2a, N1-N2a^{m1}, N1-N2a^{m2}, N1-N2a^{m4} or N1-N2a^{m6} were incubated with immobilized GST or GST-nsp3^{N}. Isolated proteins were analyzed as in panel B.

Figure 4. The *in vitro* binding defects of the doubly mutated N protein variants. (A) *Top part*. Schematic overview of the generated doubly mutated N protein variants. *Bottom part*. Bacterial extracts from *E. coli* expressing the 6×His-tagged N, N^{m4m1}, N^{m6m1}, N^{m4m2} or N^{m6m2} were incubated with immobilized GST or GST-$nsp3^{N}$. Isolated proteins were eluted by boiling in sample buffer and analyzed by western blot using the anti-6×His monoclonal antibody. GST and GST-$nsp3^{N}$ were visualized as in Fig. 1C. (B) Bacterial extracts from *E. coli* expressing the 6×His-tagged N^{m4m1} or N^{m6m1} were incubated with immobilized GST and GST-N. Isolated proteins were examined as in panel A, and GST and GST-N protein were visualized as in Fig. 1C. (C) Bacterial extract from *E. coli* expressing 6×His-tagged MHV N, N^{m4m1} or N^{m6m1} proteins were sedimented on a 15-40% glycerol gradient at 135, 000g for 75 min. Eleven fractions were collected from the top of the gel and N protein chimera distribution over the gradient was analyzed using antibodies against the 6×His tag. (D) Quantification of the immunoblots from 3 independent fractionation experiments performed as in panel C. Error bars represent SD.

Figure 5. N protein localisation to RTCs depends on its binding to nsp3. HeLa-CEACAM1a cells were transfected with plasmids expressing the GFP, GFP-N or GFP-N^{m6m1} for 48 h before to be infected or not with MHV for 7 h and processed for immunofluorescence using antibodies against MHV nsp2/3. (A) Representative images of the experiment, which and quantified in B and C. (B) The percentage of GFP-positive cells that are infected by MHV was calculated by counting the cells expressing nsp2/3 and dividing it by the number of GFP-positive. (C) The percentage of GFP-positive nsp2/3 puncta was quantified in GFP-positive cells. Scale bar, 10 µm. Error bars represent SD of 3 independent experiments. The symbol * indicates significant differences of $p<0.05$.

JVI

Figure 6. Host cells expressing N^{m6m1} mutant variant have a dominant negative effect on MHV infection. (A) HeLa-CEACAM1a cells were transfected with plasmids expressing the GFP, GFP-N or GFP-N^{m6m1} construct for 48 h and subsequently infected with the MHV-2aFLS strain at a MOI of 2.5, 5 or 10 for 7 h. In all the experiment, 80% of the cells were transfected and this was verified with a fluorescence microscope. Data represent the average luciferase activity relative to HeLa-CEACAM1a cells expressing GFP at each MOI. (B) HeLa-CEACAM1a cells were transfected as in Fig. 6A and subsequently infected with the MHV-2aFLS strain at a MOI of 5 for 5 h, 7 h or 9 h. Data represent the average luciferase activity relative to HeLa-CEACAM1a cells expressing GFP at each infection time point. (C, D) HeLa-CEACAM1a cells transfected as in Fig. 6A, were infected with MHV at MOI 5 for 5 h, 7 h or 9 h. Non-transfected cells not exposed to the virus were used as an extra control (mock). Proteins separated by SDS-PAGE were probed by western blot using antibodies recognizing MHV N protein, GFP and actin (C), and viral N protein expression was quantified and normalized to actin (D). Data depicted in panel D represent N protein amounts relative to HeLa-CEACAM1a cells expressing GFP at each infection time point. (E) Production of virus progeny in the experiment performed in Fig. 6C. Cell culture supernatants were collected at 7 h p.i. and infectious virus progeny was assessed by determining PFU per µl of supernatant. Data represent virus titers relative to HeLa-CEACAM1a cells expressing GFP at each infection time point. Error bars represent SD of 3 (C and E) or 4 (A and B) independent experiments. The symbol * indicates significant differences of $p<0.05$.

Figure 7. The N protein-nsp3 interaction induces RTCs-mediated viral RNA synthesis. (A) HeLa-CEACAM1a cells were transfected as in Fig. 6A and subsequently infected with the MHV A59 strain at a MOI of 5 for 7 h, before quantifying the amount of gRNA and sgmRNA by RT-PCR using the primer sets described in Table 1. The expression levels of gmRNA or sgmRNA were normalized to those of GAPDH, and data represent average amounts relative to the HeLa-CEACAM1a cells expressing GFP. (B) Cleared cell lysates from LR7 cells infected with MHV for 7 h (Ext) were centrifuged at 13,000×g for 10 min to obtain a pellet (P13) and a supernatant (S13) fraction. Equivalent amounts of each fraction were separated by SDS-PAGE and analyzed by western blot using antibodies against MHV N protein, VAP-A (Santa Cruz Biotechnology, Dallas, TX) and GAPDH (Fitzgerald Industries International, Acton, MA). (C) IVRS assays were performed with P13 from mock (P13) or MHV-infected (P13-MHV) cells, mixed with either the dilution buffer or the S13 from MHV-infected (S13-MHV) cells. Synthesis of viral RNA was assessed by assessing viral RNA levels by RT-PCR. Data are presented relative to those of the reaction with P13-MHV and dilution buffer. (D) The IVRS reactions were carried out with P13-MHV and S13-MHV, in presence of 0, 0.1, 1 and 2, 5 µg of bacterial lysates from *E. coli* expressing 6×His-N. gRNA levels were measured and data are presented relative to the IVRS reaction in the absence of 6×His-N. (E) The IVRS assays were carried out with P13 MHV-infected cells in presence of 1 µg of bacterial lysates from *E. coli* expressing similar levels of 6×His-N or 6×His-N^{m6m1}. This was verified prior to each experiment by western blot using and 6×His-tag antibodies. The viral RNA levels were measured and are presented relative to the control where IVRS reaction was performed in the absence of 6×His-N or 6×His-N^{m6m1}. Error bars represent SD of 3 (A, C and D) or 4 (E) independent experiments. The symbol * indicates significant differences of $p<0.05$.

JVI

Figure 8. The role of CoV N or N^{m6m1} proteins at the viral replication platforms. Upon synthesis, CoV N or N^{m6m1} proteins constitutively assemble into cytoplasmic oligomers. The wild type N oligomers are recruited via the interaction with nsp3 to the RTCs that are localized on DMVs and convoluted membranes. There, the N oligomers stimulate gRNA and sgmRNA synthesis. It may also be presence of N oligomers at the RTCs promotes local formation of ribonucleoprotein complexes. In contrast, the inability of N^{m6m1} protein to be recruited to the RTCs severely impairs transcription, replication and ultimately virion production.

TABLE 1 Primer sets used for the specific quantification of gRNA and sgmRNA by RT-PCR

Primer name	Primer sequence (5' to 3')	Remark
481F 620R	GCCTCAACTATGATGGCATT AGAGCACTCCCGAAGAGGAC	gRNA
21886R 19 F	GTCTAAACCCATTTCCACA TCCGTACGTACCCTCTCAACTCTAA	sgmRNA1 (NS2a)
24031R 19 F	TCTCAGTGCTAATGCTTGGA TCCGTACGTACCCTCTCAACTCTAA	sgmRNA2 (S)
28397R 19 F	GCATCATCACATGCCAAAT TCCGTACGTACCCTCTCAACTCTAA	sgmRNA3 (ORF5)
29091R 19 F	GGCTCGTGTAACCGAACTGT TCCGTACGTACCCTCTCAACTCTAA	sgmRNA4 (M)
GAPDH_F GAPDH_R	AGCCACATCGCTCAGACAC GCCCAATACGACCAAATCC	Internal control
27379F 27501R	TGGAGAATGGAAGTTCACAGG GTCGGGTGGATTAGGTATTGAAG	Viral mRNA (S)

JVI

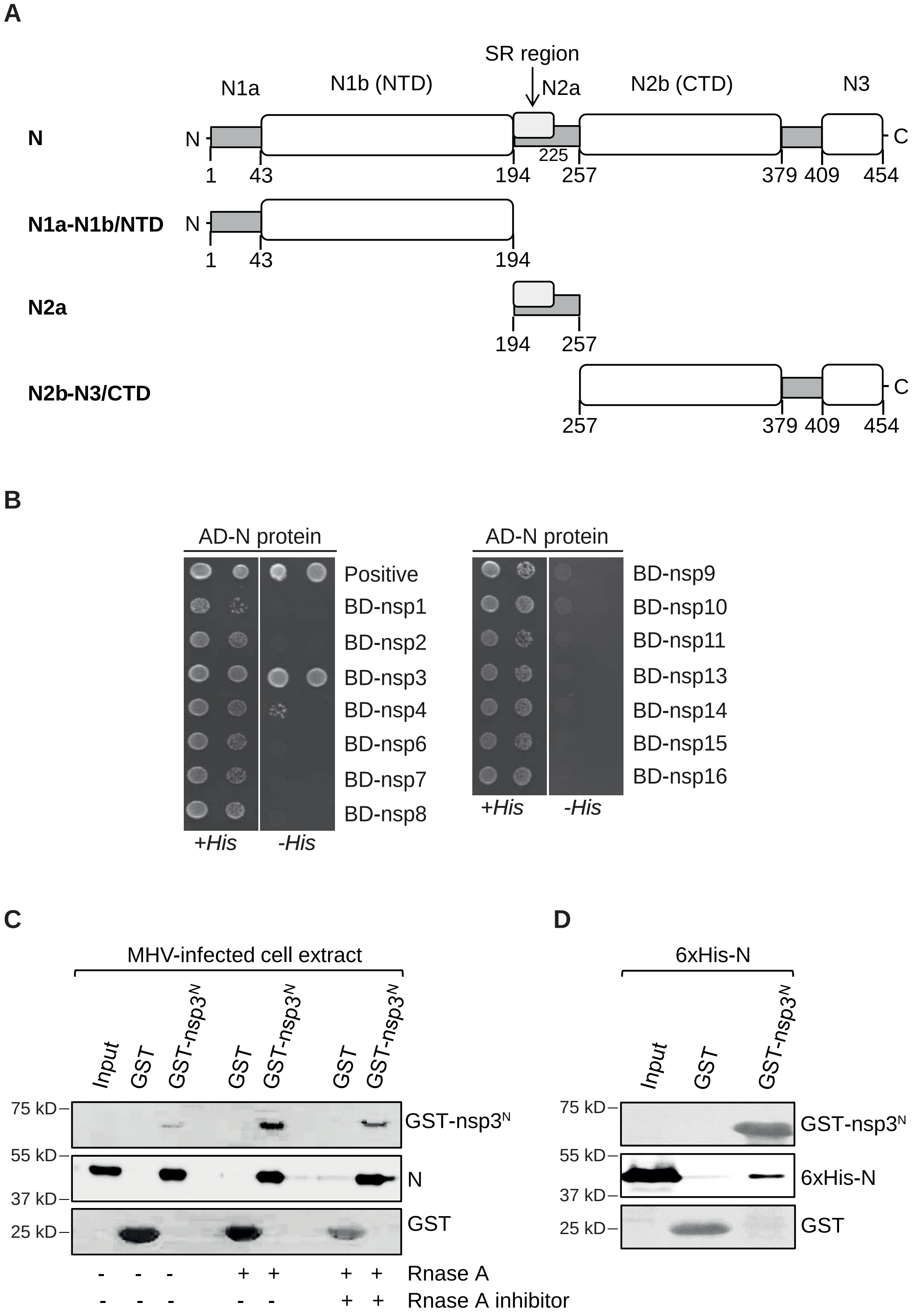

Cong et al, Figure 1

JVI

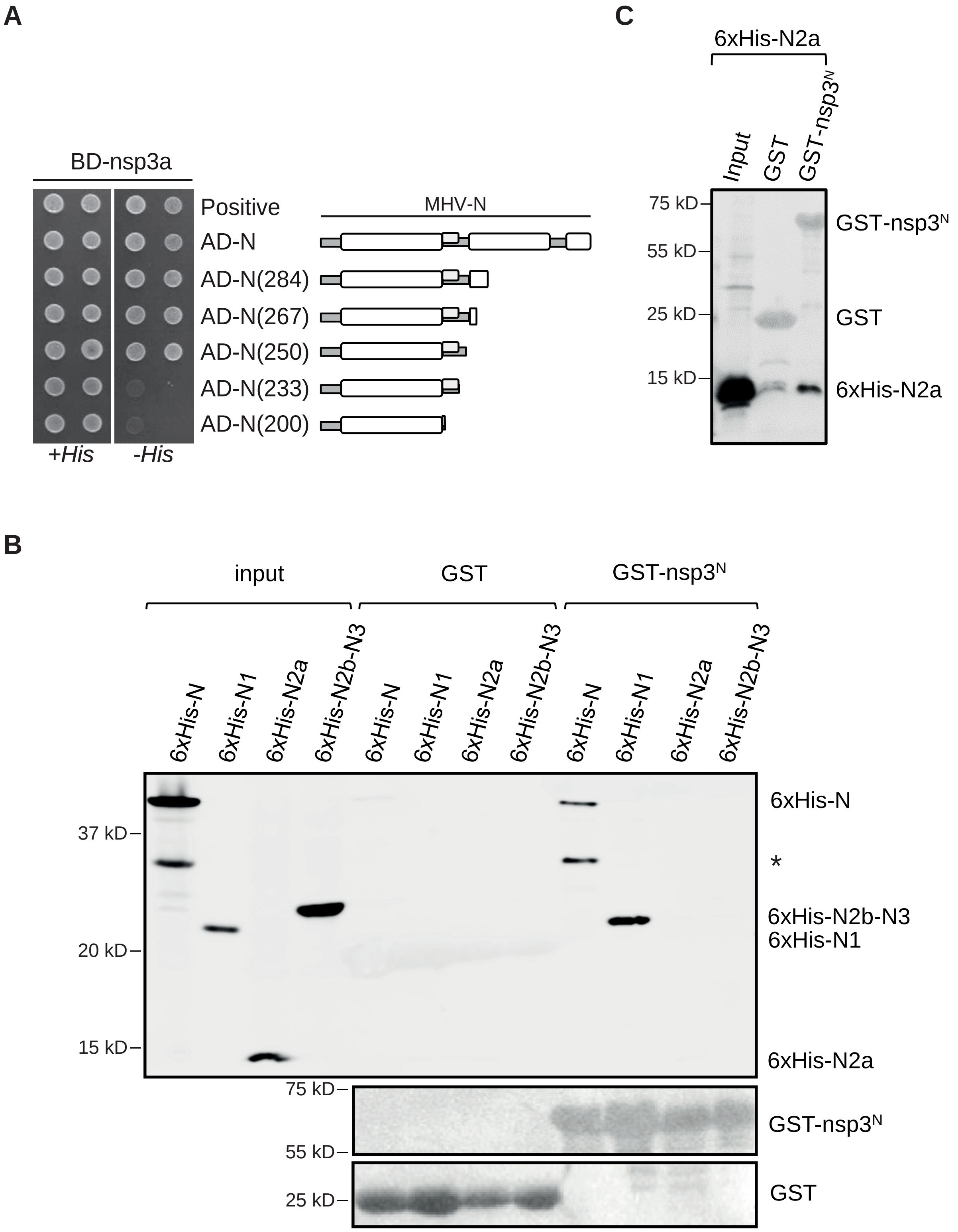

Cong et al, Figure 2

JVI

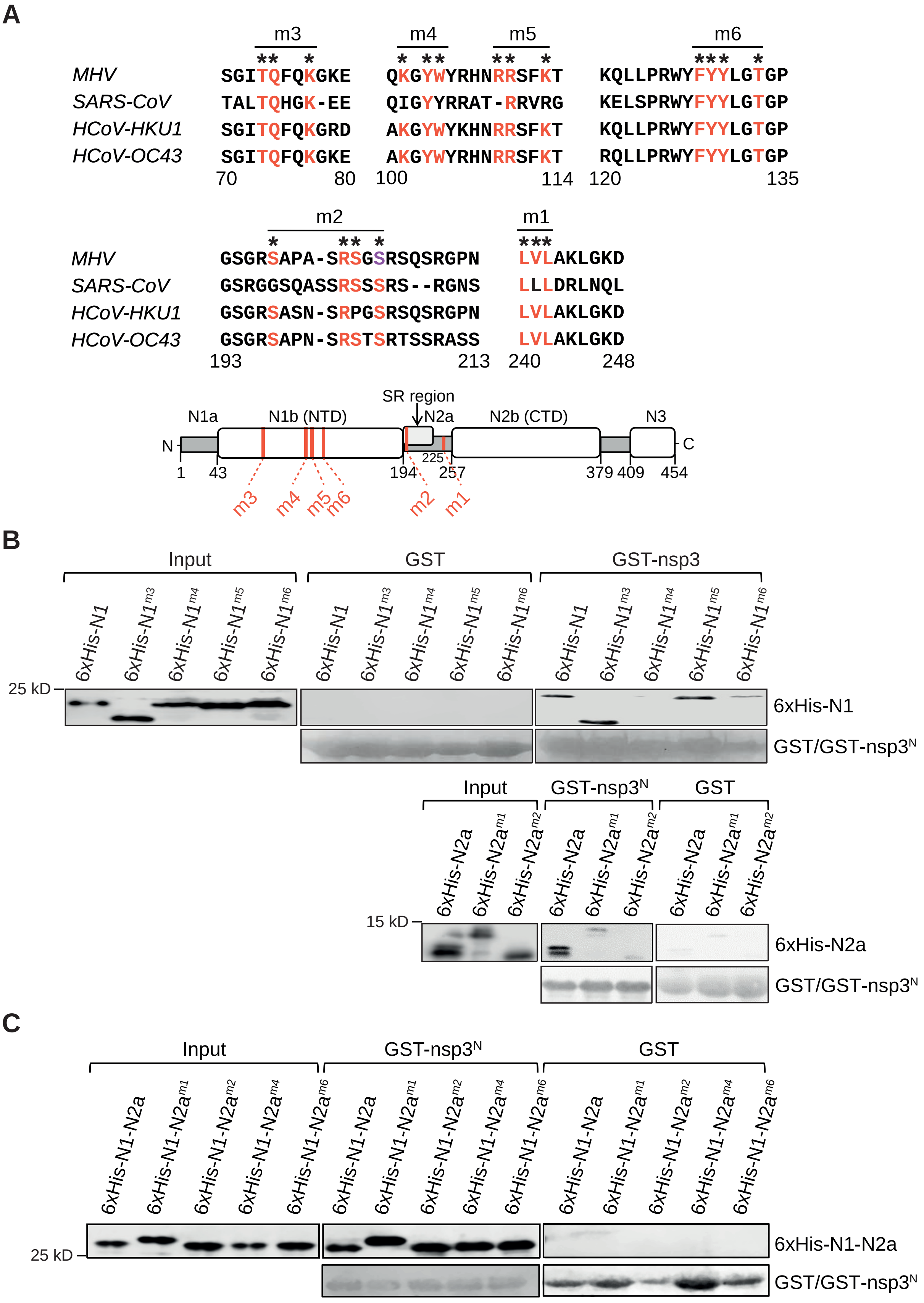

Cong et al, Figure 3

JVI

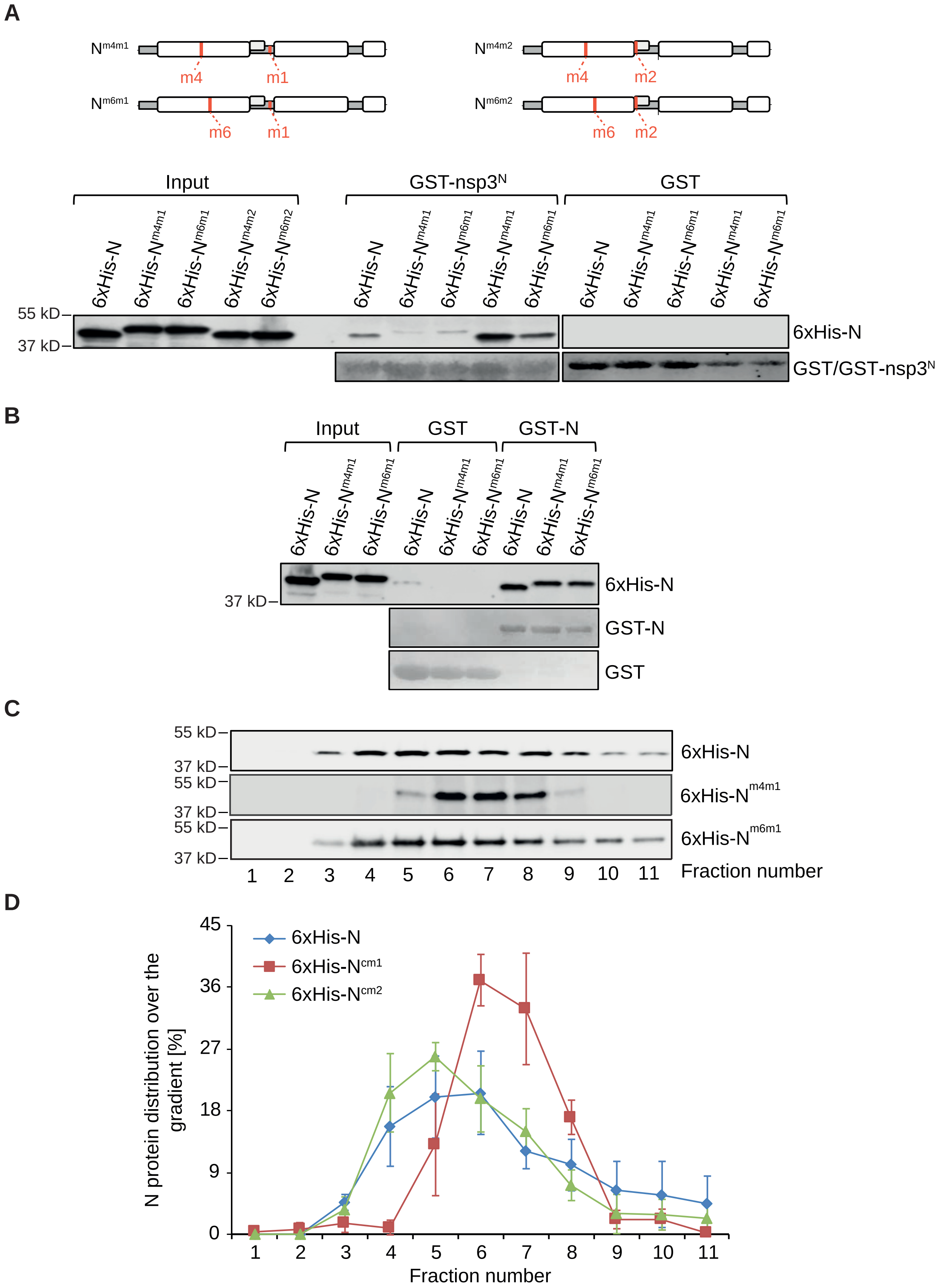

Cong et al, Figure 4

JVI

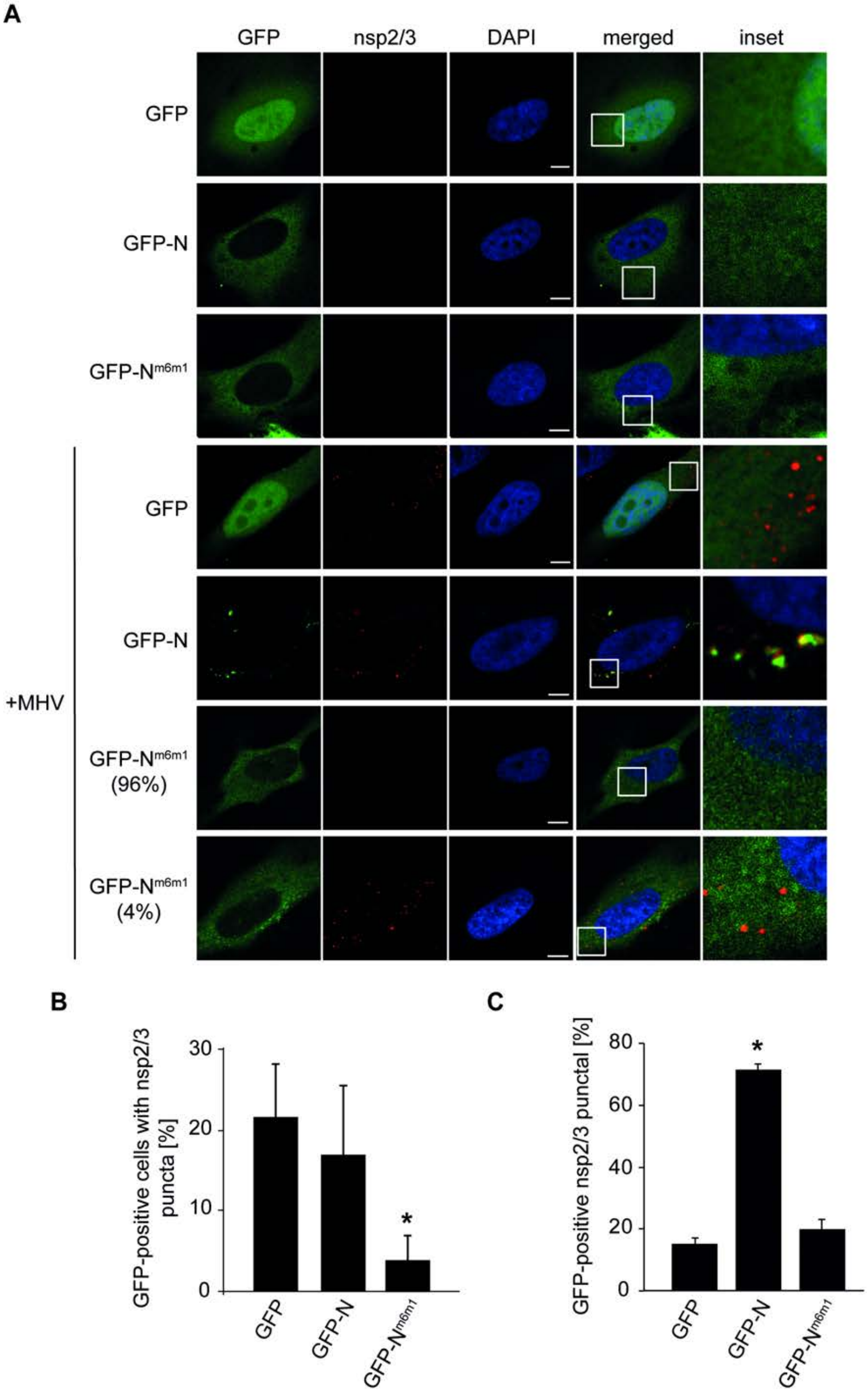

Cong et al, Figure 5

JVI

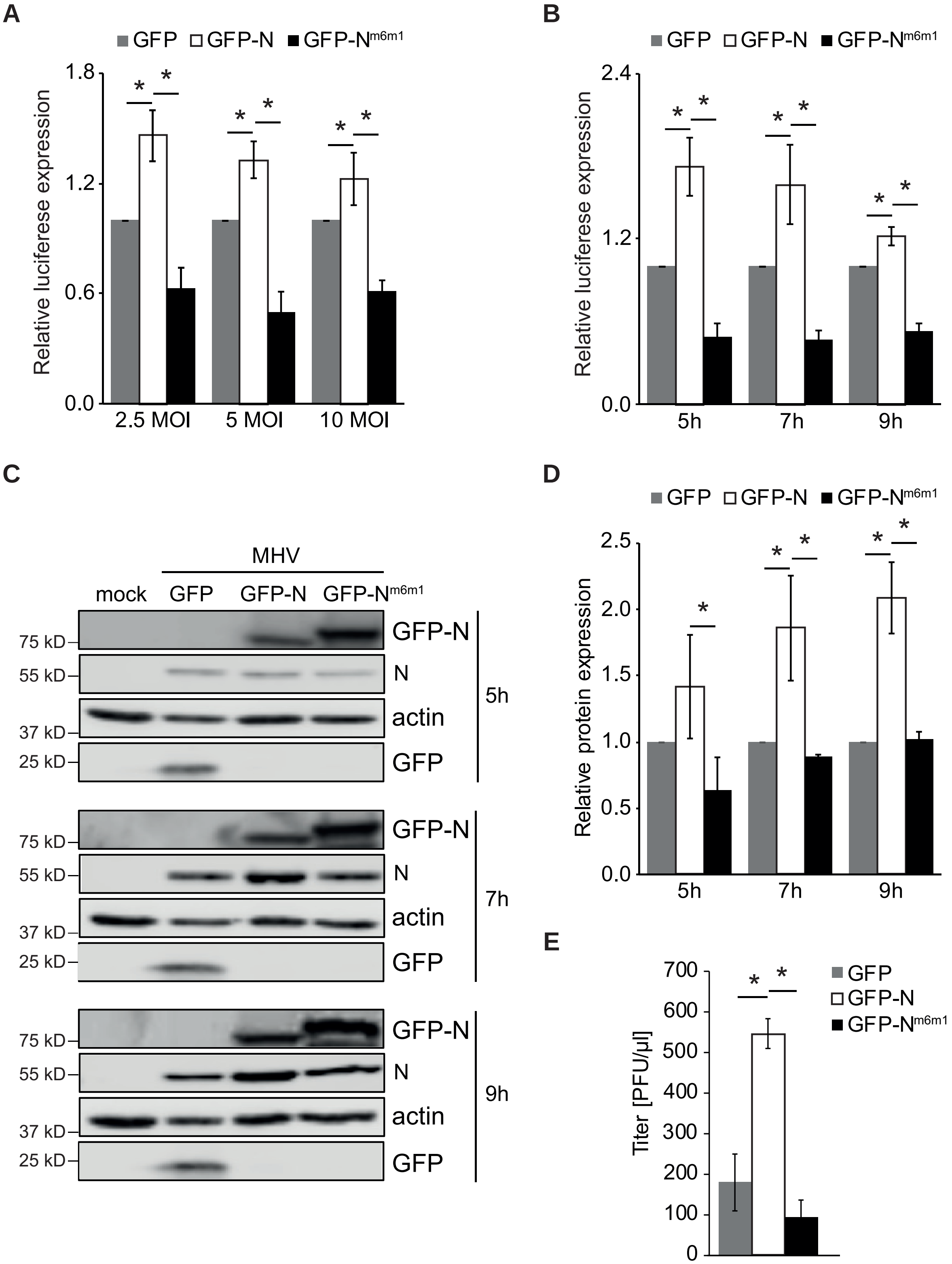

Cong et al, Figure 6

JVI

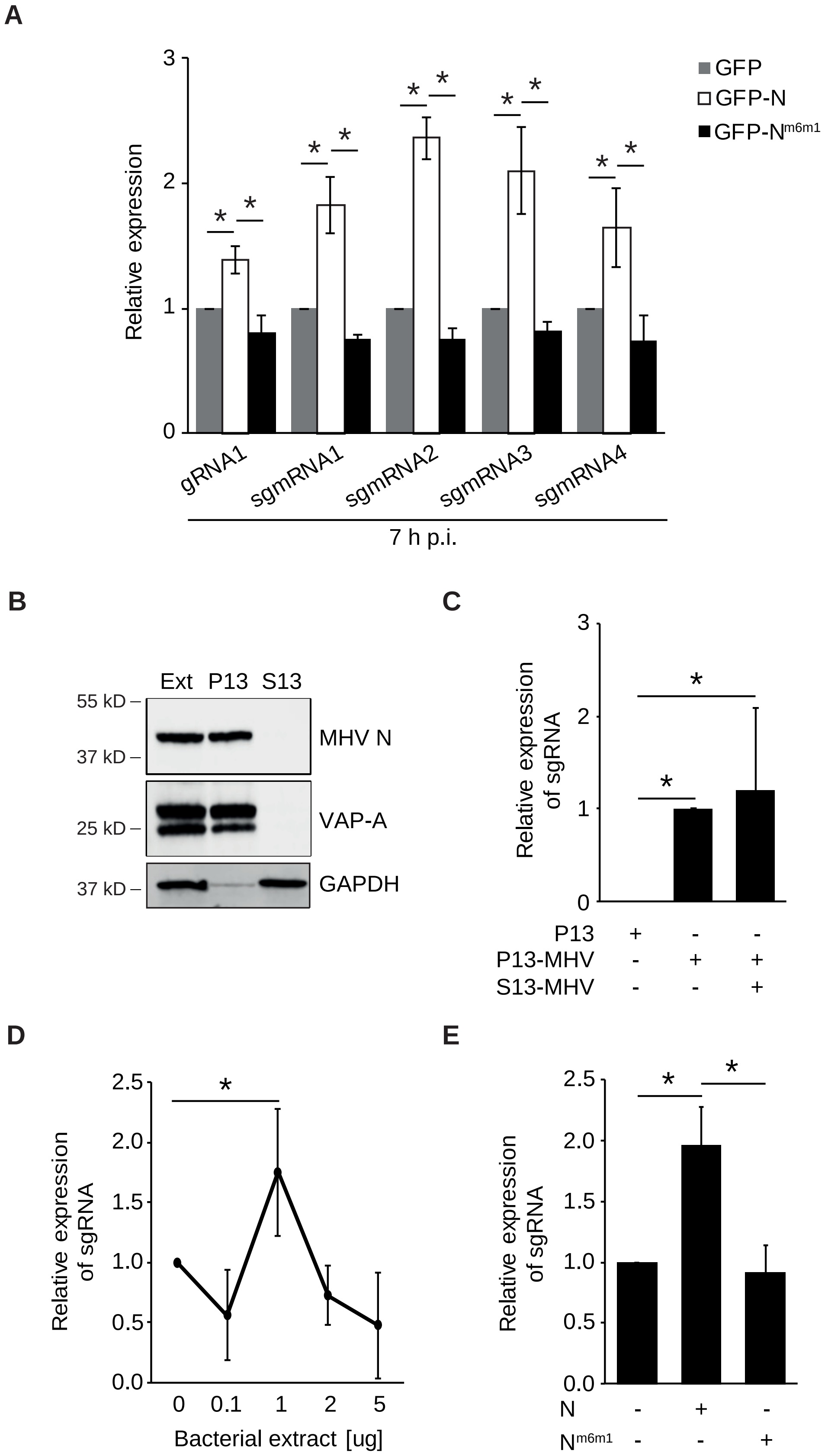

Cong et al, Figure 7

JVI

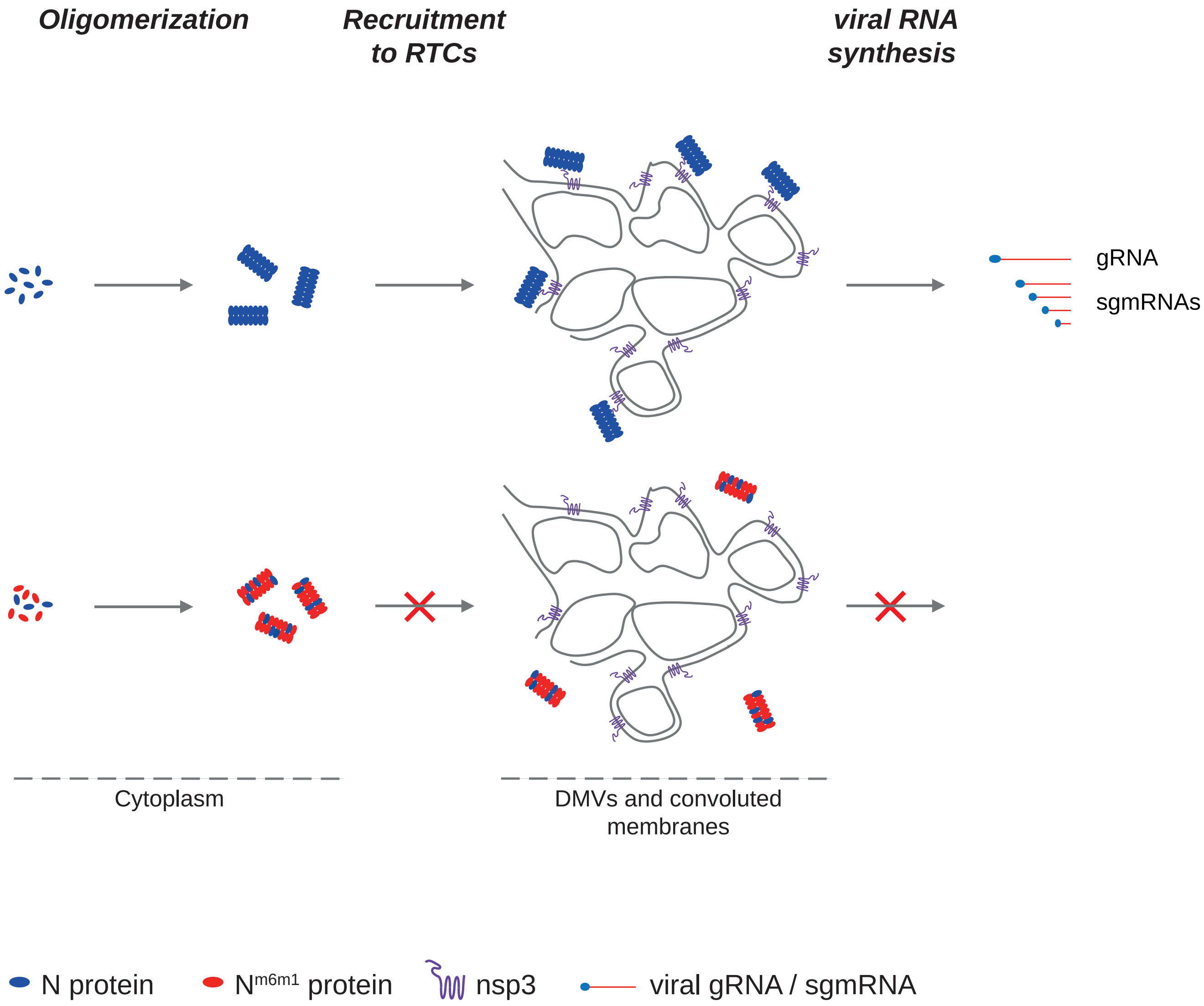

Cong et al, Figure 8